NOAA Technical Report NESS 74

On the Estimation of Areal Windspeed Distribution in Tropical Cyclones With the Use of Satellite Data

Washington, D.C.
August 1976

U.S. DEPARTMENT OF COMMERCE
National Oceanic and Atmospheric Administration
National Environmental Satellite Service

NOAA TECHNICAL REPORTS

National Environmental Satellite Service Series

The National Environmental Satellite Service (NESS) is responsible for the establishment and operation of the environmental satellite systems of NOAA.

Publication of a report in NOAA Technical Report NESS series will not preclude later publication in an expanded or modified form in scientific journals. NESS series of NOAA Technical Reports is a continuation of, and retains the consecutive numbering sequence of, the former series, ESSA Technical Report National Environmental Satellite Center (NESC), and of the earlier series, Weather Bureau Meteorological Satellite Laboratory (MSL) Report. Reports 1 through 39 are listed in publication NESC 56 of this series.

Reports 1 through 50 in the series are available from the National Technical Information Service (NTIS), U.S. Department of Commerce, Sills Bldg., 5285 Port Royal Road, Springfield, Va. 22151, in paper copy or microfiche form. Order by accession number, when given, in parentheses. Beginning with 51, printed copies of the reports are available through the Superintendent of Documents, U.S. Government Printing Office, Washington, D.C. 20402; microfiche available from NTIS (use accession number when available). Prices given on request from the Superintendent of Documents or NTIS.

ESSA Technical Reports

NESC 41 The SINAP Problem: Present Status and Future Prospects; Proceedings of a Conference Held at the National Environmental Satellite Center, Suitland, Maryland, January 18-20, 1967. E. Paul McClain, October 1967, 26 pp. (PB-176-570)

NESC 42 Operational Processing of Low Resolution Infrared (LRIR) Data From ESSA Satellites. Louis Rubin, February 1968, 37 pp. (PB-178-123)

NESC 43 Atlas of World Maps of Long-Wave Radiation and Albedo--for Seasons and Months Based on Measurements From TIROS IV and TIROS VII. J. S. Winston and V. Ray Taylor, September 1967, 32 pp. (PB-176-569)

NESC 44 Processing and Display Experiments Using Digitized ATS-1 Spin Scan Camera Data. M. B. Whitney, R. C. Doolittle, and B. Goddard, April 1968, 60 pp. (PB-178-424)

NESC 45 The Nature of Intermediate-Scale Cloud Spirals. Linwood F. Whitney, Jr., and Leroy D. Herman, May 1968, 69 pp. plus appendixes A and B. (AD-673-681)

NESC 46 Monthly and Seasonal Mean Global Charts of Brightness From ESSA 3 and ESSA 5 Digitized Pictures, February 1967-February 1968. V. Ray Taylor and Jay S. Winston, November 1968, 9 pp. plus 17 charts. (PB-180-717)

NESC 47 A Polynomial Representation of Carbon Dioxide and Water Vapor Transmission. William L. Smith, February 1969 (reprinted April 1971), 20 pp. (PB-183-296)

NESC 48 Statistical Estimation of the Atmosphere's Geopotential Height Distribution From Satellite Radiation Measurements. William L. Smith, February 1969, 29 pp. (PB-183-297)

NESC 49 Synoptic/Dynamic Diagnosis of a Developing Low-Level Cyclone and Its Satellite-Viewed Cloud Patterns. Harold J. Brodrick and E. Paul McClain, May 1969, 26 pp. (PB-184-612)

NESC 50 Estimating Maximum Wind Speed of Tropical Storms From High Resolution Infrared Data. L. F. Hubert, A. Timchalk, and S. Fritz, May 1969, 33 pp. (PB-184-611)

NESC 51 Application of Meteorological Satellite Data in Analysis and Forecasting. Ralph K. Anderson, Jerome P. Ashman, Fred Bittner, Golden R. Farr, Edward W. Ferguson, Vincent J. Oliver, Arthur H. Smith, James F. W. Purdom, and Rance W. Skidmore, March 1974 (reprint and revision of NESC 51, September 1969, and inclusion of Supplement, November 1971, and Supplement 2, March 1973), pp. 1--6C-18 plus references.

NESC 52 Data Reduction Processes for Spinning Flat-Plate Satellite-Borne Radiometers. Torrence H. MacDonald, July 1970, 37 pp. (COM-71-00132)

NESC 53 Archiving and Climatological Applications of Meteorological Satellite Data. John A. Leese, Arthur L. Booth, and Frederick A. Godshall, July 1970, pp. 1-1--5-8 plus references and appendixes A through D. (COM-71-00076)

(Continued on inside back cover)

NOAA Technical Report NESS 74

On the Estimation of Areal Windspeed Distribution in Tropical Cyclones With the Use of Satellite Data

Andrew Timchalk
Meteorological Satellite Laboratory
National Environmental Satellite Service
NOAA, Washington D.C.

Washington, D.C.
August 1976

U.S. DEPARTMENT OF COMMERCE
Elliot L. Richardson, Secretary

National Oceanic and Atmospheric Administration
Robert M. White, Administrator

National Environmental Satellite Service
David S. Johnson, Director

This paper is a modified version of a thesis submitted to the faculty of the Graduate School of the University of Maryland in partial fulfillment of the requirements for the degree of Master of Science (1975)

CONTENTS

Tables

Figures

ACRONYMS, SYMBOLS, AND ABBREVIATIONS

GMT	Greenwich Meridian Time
NESS	National Environmental Satellite Service
NOAA	National Oceanic and Atmospheric Administration
SMS	Synchronous Meteorological Satellite
SRIR	Scanning Radiometer InfraRed
Tiros	Television and Infrared Observation Satellite
a	Intercept of regression line
b	Slope of regression line
kt	Knots
n,N	Sample size
R	Radius (in degrees of latitude; 1° = 60 n.mi.)
(r)	Linear correlation coefficient
S	Standard error about the regression line
T_{BB}	Infrared temperature in degrees Kelvin
μm	Micrometer
v, v_{obs}	Observed windspeed in knots
$\bar{v}_{obs}$	Mean algebraic value of observed windspeed in knots
$\lvert\bar{v}_{obs}\rvert$	Mean absolute value of observed windspeed in knots
$\Delta v/\Delta\Theta$	Tangential variation of windspeed (kt per $\pi/8$ radians)
$\Delta v/\Delta R$	Radial variation of windspeed (kt per degree latitude)
α	Crossing angle (degrees) with respect to tangents to concentric circles centered on the eye
α_{cld}	Crossing angle of low-level convective cloud bands
α_{obs}	Crossing angle of the observed wind direction
α_{rel}	Crossing angle of the relative wind direction
v_θ	Tangential wind velocity
v_r	Radial wind velocity

ON THE ESTIMATION OF AREAL WINDSPEED DISTRIBUTION IN TROPICAL CYCLONES WITH THE USE OF SATELLITE DATA

Andrew Timchalk
Meteorological Satellite Laboratory
National Environmental Satellite Service
NOAA, Washington, D.C.

ABSTRACT. This paper is an attempt to determine whether the areal windspeed distributions in tropical cyclones can be estimated by use of two satellite data parameters: (1) the low-level convective cloud band crossing angle relative to tangents to concentric circles centered on the eye, (2) the infrared temperatures from the 10.5-to-12.5 μm channel. These two parameters plus the "ground truth" winds were all derived for 128 polar coordinate grid points (16 azimuths and 8 radii).

Coincident values of the variables were evaluated statistically first by linear regression and afterward by multiple screening regression. For the entire storm area (all radii), the correlation between observed windspeed and the two satellite-derived parameters [(1) and (2), above] was 0.4 and -0.6, respectively. However, when evaluated at separate radii the two satellite parameters were poorly correlated to either the observed or relative windspeed.

Radial distance from the storm center was found to explain 63% of the variance in windspeed. When this relation was removed by screening regression, the two satellite parameters could explain only an additional 2% to 3% of the variance.

Correlation between the cloud band crossing angle and the wind field crossing angle was less than 0.5 at all radii. Correlation between the windspeed and the wind field crossing angle was less than 0.2. In both cases, the coefficients were lower than expected.

I. INTRODUCTION

A. Problem and Scope

The purpose of this work is to determine whether the areal windspeed distributions in tropical cyclones can be estimated using satellite data parameters. The scope of this study is confined to two such parameters. Low-level convective cloud band crossing angles relative to tangents to

concentric circles centered on the eye were obtained from the 0.5-to-0.7 μm visual channel and infrared brightness temperatures from the 10.5-to-12.5 μm infrared channel.

Because of expected vertical wind shear at radii beyond 100 n.mi. from a storm center, aerial reconnaissance winds are probably unrepresentative of winds near the surface. Therefore, this study was designed to estimate the distribution of the maximum sustained windspeed at ship deck level. Satellite parameters and windspeeds were derived over a 128-point polar coordinate grid consisting of points located at 16 azimuth angles and 8 radii from storm center.

B. Past Studies of Wind Distribution

Prior to 1943, when the military services of the United States began aerial reconnaissance into tropical cyclones, practically all the data used for the study of wind distributions in storms were measured at island and coastal stations. Based on empirical observations indicating that angular momentum was only partially conserved, Byers (1944) predicted that the windspeed should be inversely proportional to the square root of the radial distance from the storm center. Similar wind structure in tropical cyclones has since been noted by numerous investigators.

The "classical" model of the wind field surrounding tropical cyclones was developed by Hughes (1952). By using low-level (about 1,000 feet) reconnaissance data for the period 1945-47, Hughes derived a typical windspeed distribution for a large, stationary, mature cyclone. Hughes found that when he substituted the tangential windspeeds at radii 1° and 3° (60 and 180 n.mi.) into the equation:

$$v_\theta R^x = C \qquad (1)$$

(where R is the radius, v_θ the tangential windspeed, C and x are constants), x = 0.62 provided the best fit. This compares with the 0.5 predicted by Byers (1944) and Riehl (1963).

Jordan (1952) constructed a picture of the upper-level wind circulation around tropical cyclones. Miller (1958) investigated the three-dimensional wind structure around hurricanes. Hawkins (1962) examined the vertical profiles of horizontal wind in hurricanes and found that the preservation of the windspeed with height is well-marked below 20,000 feet within a radius 2.5 times the radius of maximum winds. These and similar studies have not only provided data, but have also served as a basis for many subsequent theoretical and experimental studies.

A search of the literature shows that most studies of wind distributions are either of individual storm cases or are of the high energy core of the storms; that is, within radii of less than 100 n.mi. from the storm center. This limitation is mainly due to the lack of low-level aircraft reconnaissance beyond the 100 n.mi. (Shea and Gray 1972).

C. Need for the Study

Knowledge of the low-level windspeed in tropical cyclones is important for the safety of all ocean going vessels. The areal distribution of windspeed, e.g., the extent of the 30- and 50-kt isotachs is important in preparedness or evacuation decisions for coastal installations (Brand and Blelloch 1975). Distributions of windspeed and inflow angle affect the height of storm surges that accompany intense tropical cyclones (Jelesnianski 1966); and areal speed distributions are of primary importance in the study of the dynamics and energetics of these storms.

Weather satellite capability to view large, remote areas of the tropics simultaneously, and the increasing cost of aircraft reconnaissance, are compelling reasons to search for methods of specifying the windspeed in tropical cyclones.

Satellite data are being used effectively to locate, and to estimate the maximum intensity of, tropical cyclones (Sheets and Grieman 1975); however, little study has been devoted to the use of these data in specifying the areal distribution of the windspeed in storms.

II. METHOD

A. Selection of Satellite Data Parameters

1. Selection of Cloud Band Crossing Angle.

A hurricane is a thermally driven circulation whose primary energy source is the release of latent heat of condensation. A model hurricane shows a wind field with cyclonic inflow in the lower troposphere and anticyclonic outflow aloft. Riehl (1963) obtained some reasonable results from a simple two-layer model he developed in which the storm is assumed to be symmetrical and steady-state. Conservation of absolute angular momentum in the outflow layer and conservation of potential vorticity in the inflow layer were the key assumptions.

Through the use of the absolute angular momentum equation, the equation for the tangential component of motion, and assuming conservation of potential vorticity in the inflow layer, Riehl derived an expression for the tangential windspeed distribution in tropical cyclones eq. (11). His initial formulation contained an inflow angle term ($\cos \alpha$), where α is the angle the wind makes with a tangent to a circle centered on the storm. This term was later omitted after applying the findings of Ausman (1959) because the value of $\cos \alpha$ was near unity when the crossing angles were small (i.e., nearly tangential flow). However, this term will be retained following the derivation of Riehl (1963).

The equation of motion in polar coordinates for the tangential component, neglecting lateral friction, is:

$$\frac{dv_\theta}{dt} + \frac{v_\theta v_r}{R} + fv_r = - \frac{1}{\rho}\frac{\partial P}{\partial \theta} + \frac{1}{\rho}\frac{\partial T_{\theta z}}{\partial z}, \qquad (2)$$

where v_θ is the tangential velocity, v_r the radial velocity, and $T_{\theta z}$ the tangential shearing stress in the θ-z plane. The absolute angular momentum per unit mass about a vertical axis at the storm center is given by:

$$\Omega = v_\theta R + \frac{fR^2}{2} . \qquad (3)$$

Differentiating eq. (3) with respect to time and noting that $dR/dt = v_r$, yields:

$$\frac{d\Omega}{dt} = R\frac{dv_\theta}{dt} + v_\theta v_r + Rfv_r . \qquad (4)$$

Multiplying eq. (2) by R, eq. (4) can be written as:

$$\frac{d\Omega}{dt} = - \frac{R}{\rho}\frac{\partial P}{\partial \theta} + \frac{R}{\rho}\frac{\partial T_{\theta z}}{\partial z} . \qquad (5)$$

Assuming a symmetric vortex, $\partial P/\partial \theta = 0$, so

$$\frac{d\Omega}{dt} = \frac{R}{\rho}\frac{\partial T_{\theta z}}{\partial z} . \qquad (6)$$

Eq. (6) shows that the time rate of change of absolute angular momentum depends on the vertical gradient of the shearing stress.

For the inflow layer, eq. (6) can be integrated over an inflow depth of δz where at the top, $T_{\theta z} = 0$.

$$\int \frac{d\Omega}{dt}\rho\delta z = -T_{\theta s} , \qquad (7)$$

where $T_{\theta s}$ is the surface tangential shearing stress. Assuming conservation of potential vorticity, the curl of the component of frictional force along θ must be zero. That is, $\nabla \times F_\theta = 0$ where

$F_\theta = \frac{1}{\rho}\frac{\partial T_{\theta z}}{\partial z}$. Thus for $F_\theta R$ = constant (and by integrating from the surface

to the height where the stress vanishes) the result is:

$$RT_{\theta s} = \text{constant} . \tag{8}$$

At this point an empirically derived expression for the surface stress is introduced:

$$T_{\theta s} = C_d \rho_s v_\theta^2 / \cos \alpha . \tag{9}$$

C_d is the drag coefficient, ρ_s the surface density, $v_{\theta s}$ the surface tangential windspeed (at ship deck level) and α is the inflow or crossing angle.

Combining eq. (8) and (9) and solving for $v_{\theta s}$:

$$v_{\theta s} = C_1 (\cos \alpha / R)^{\frac{1}{2}} , \tag{10}$$

where $C_1 = (\text{constant}/C_d \rho_s)^{\frac{1}{2}}$. Eq. (10) shows that the tangential windspeed is directly proportional to the square root of cos α. Hence, windspeed is inversely related to the crossing angle. Note that when the flow is tangential, i.e., $\alpha = 0$, cos $\alpha = 1$. Thus eq. (10) reduces to the well-known tangential windspeed distribution equation where the subscript (s) has been omitted for convenience:

$$v_\theta R^{\frac{1}{2}} = C_1 . \tag{11}$$

For convenience also, eq. (11) will be written in the form:

$$v_\theta = C_1 R^{-0.5} . \tag{12}$$

In hurricanes the tangential component of the windspeed (v_θ) is usually much larger than the radial component (v_r); therefore the total windspeed should be closely approximated by the tangential component. Further, if the cloud bands are alined with the wind direction, then as indicated by eq. (10), the observed wind speed should be directly proportional to the square root of the cosine of the low cloud band crossing angle. The relation implied by eq. (10) along with satellite studies by Timchalk et al. (1965), Fritz et al. (1966), and Dvorak (1973) were the bases for selecting the crossing angle of cloud bands (α_{cld}) as one of the satellite data parameters. A necessary assumption is that α_{cld} is nearly equal to the crossing angle of the observed wind (α_{obs}); this assumed relation will also be examined.

2. Selection of Infrared Radiation Temperature

Riehl (1954), citing high-level observations and the theoretical work of Haurwitz (1935), noted that mature storms extend through the troposphere to near the 100-mb level. At these levels, the cloud-top temperatures would be as low as -78°C (Schacht 1946). Accordingly, very cold cloud-top temperatures should be found over intense storms.

The work of Fritz et al. (1966) with the TIROS visible channel data showed a positive correlation between the size of the hurricane "canopy" and the maximum windspeed in tropical cyclones. Further, in an attempt to establish a relation between the equivalent blackbody radiation temperature (T_{BB}) and the intensity of tropical cyclones, Hubert et al. (1969) found the canopy sizes could be closely approximated by the extent of the 260 K infrared isotherms. They noted that T_{BB} at the wall cloud radius, where the maximum windspeeds are located, was in most cases colder than 230 K, while in the outer areas, where the windspeeds are low, T_{BB} was near 300 K. These findings suggested that windspeed should be inversely related to T_{BB}, particularly over intense tropical cyclones. Because satellite infrared temperature had been observed to be related to the windspeed, T_{BB} was selected as a study parameter.

B. Analysis

1. Determination of Wind Field

Since the objective of this study was to estimate the areal windspeed distribution, it was necessary to obtain the "ground truth" wind field. Following the recommendation of Frank (1974), aircraft reconnaissance data were collected via the Navy's Hurricane Circuit located at the Fleet Weather Central Suitland, Md. over the Atlantic Ocean during the 1974 tropical storm season. Aircraft reports at or below the 700-mb level, rawinsonde wind data for the 609-m level, and ship and buoy data, were used. The 609-m level was chosen after noting the work of Hawkins (1962) and examining vertical profiles of windspeed.

All the data were composited about the 1600 GMT position of the storm. To do this, the bearing and distance from the storm center of each observation was calculated from the interpolated storm position. The observations for each day were then plotted on a Mercator projection showing the wind direction, speed, type and height of wind observation, and the time difference from 1600 GMT. Only wind observations that were made within $\pm$ 8 hours of 1600 GMT were used.

Applying the results of Riehl (1954), Miller (1958), Hawkins (1962), and others, isogon/streamline and isotach analyses were made, considering such factors as type, height, and reliability of wind observation coupled with time and spatial consistency. These field analyses were used to extract the wind direction and speed for the polar coordinate grid at 16 azimuth angles and radial increments of 1° latitude (60 n.mi.) outward to a distance of 8° latitude (480 n.mi.) from the storm center.

Figure 1 shows the isogon-streamline analysis and figure 2 shows the isotach analysis for hurricane Carmen on Sept. 1, 1974. From these analyses, wind direction and speed were extracted at each of the 128 grid points shown in figure 3. Wind fields were prepared for 10 days selected from 3 hurricanes. Copies of the wind field may be obtained by contacting the author.

Since none of the 10 storm cases was stationary over the 16-hour composite period, smoothed track positions were used to calculate a mean storm motion vector which is printed at the center of the polar grid for each case. The first three digits indicate the azimuth toward which the storm was moving, while the remaining two digits indicate the speed of translation in knots. A list of the storm cases, dates, positions, and storm motion vectors used in this study is given in table 1.

Table 1.--List of storm cases

Hurricane	Date	Location at 1600 GMT	Storm motion vector direction/speed(kt)
Carmen	9/01/74	17.6N 83.9W	274/13
"	9/02/74	18.8N 88.7W	280/10
"	9/05/74	21.5N 90.7W	010/04
"	9/06/74	23.5N 90.4W	008/09
"	9/07/74	27.5N 90.4W	360/10
"	9/08/74	30.3N 92.5W	320/10
Fifi	9/17/74	16.9N 80.8W	260/08
"	9/18/74	16.3N 84.3W	270/15
"	9/19/74	16.1N 88.0W	290/08
Camille	8/17/69	27.5N 88.5N	344/12

In moving storms, the wind at a given point contains both rotational and translational components. If the translation component (the storm motion vector) is subtracted vectorially from the wind at each grid point, the new field is called the "relative" wind field. Both the observed and relative wind fields were studied for possible relations with the two satellite parameters. An example of the relative wind field for hurricane Carmen on Sept. 1, 1974 is shown in figure 4. Comparison of figures 3 and 4 shows the difference between the relative and the observed wind fields for a storm moving toward the west at 13 kt.

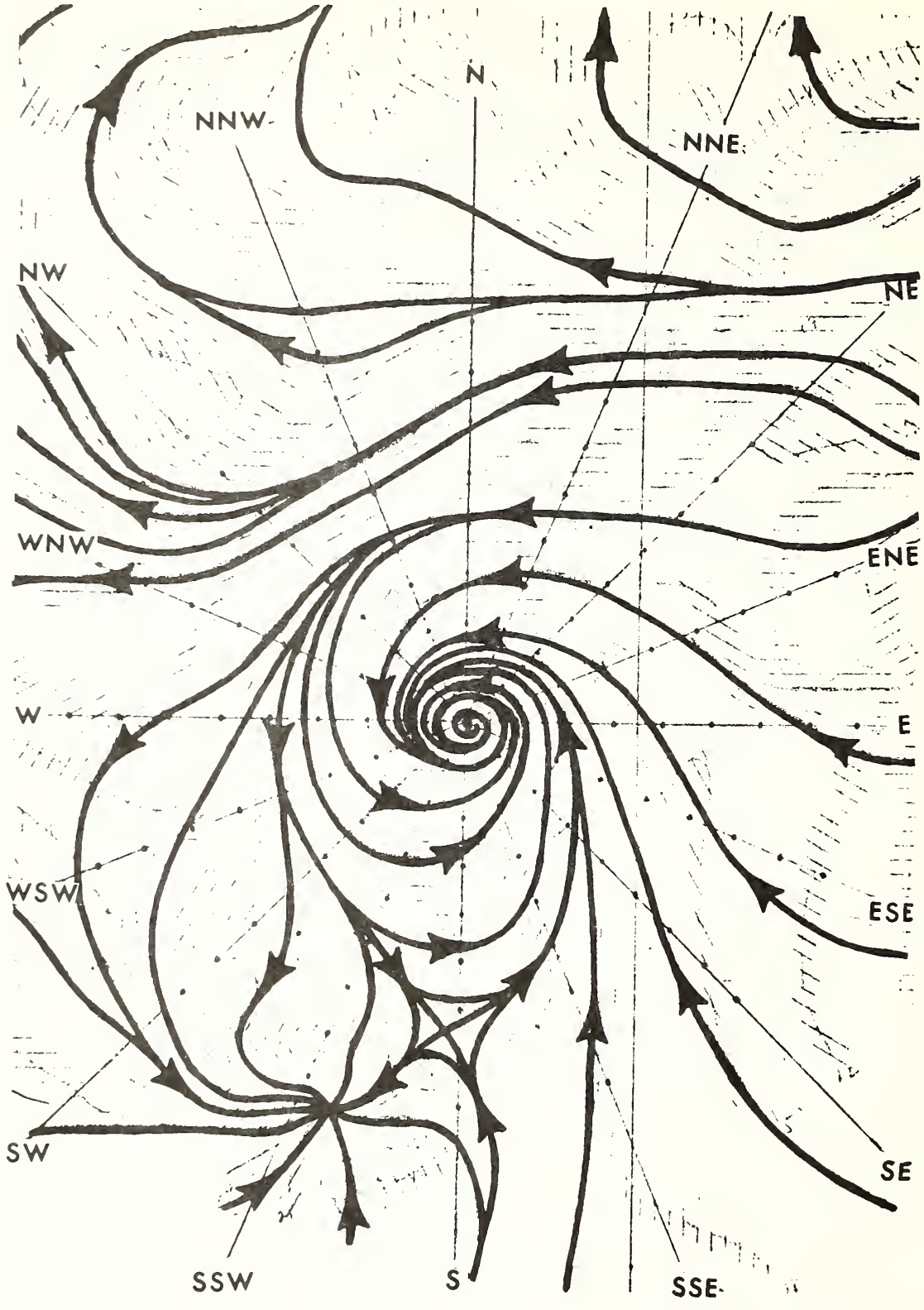

Figure 1.--Isogon-streamline analysis for hurricane Carmen, 1600 GMT, Sept. 1, 1974. Eye position: 17.6N, 83.9W.

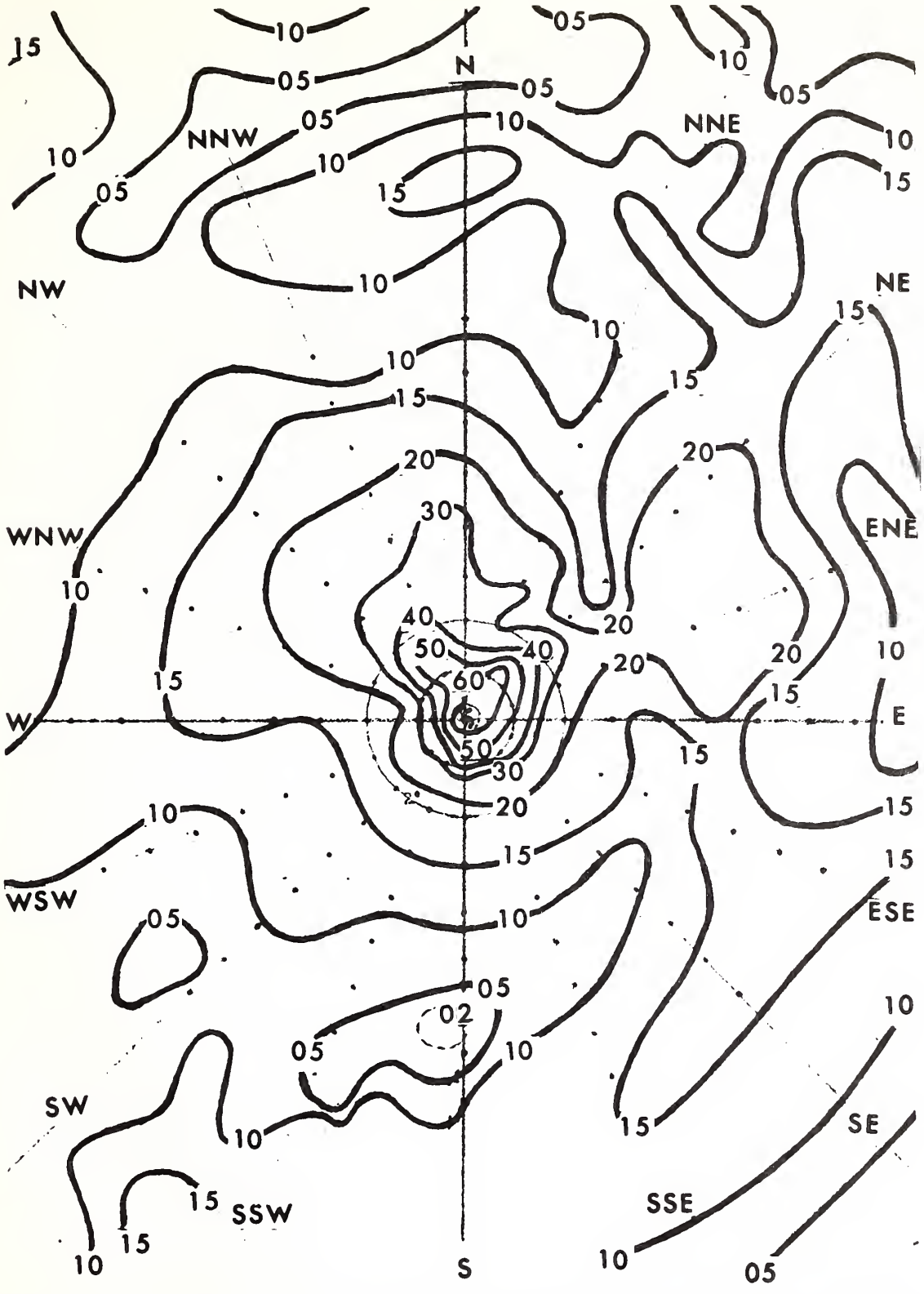

Figure 2.--Isotach analysis (kt) for hurricane Carmen, 1600 GMT, Sept. 1, 1974. Eye position: 17.6N, 83.9W.

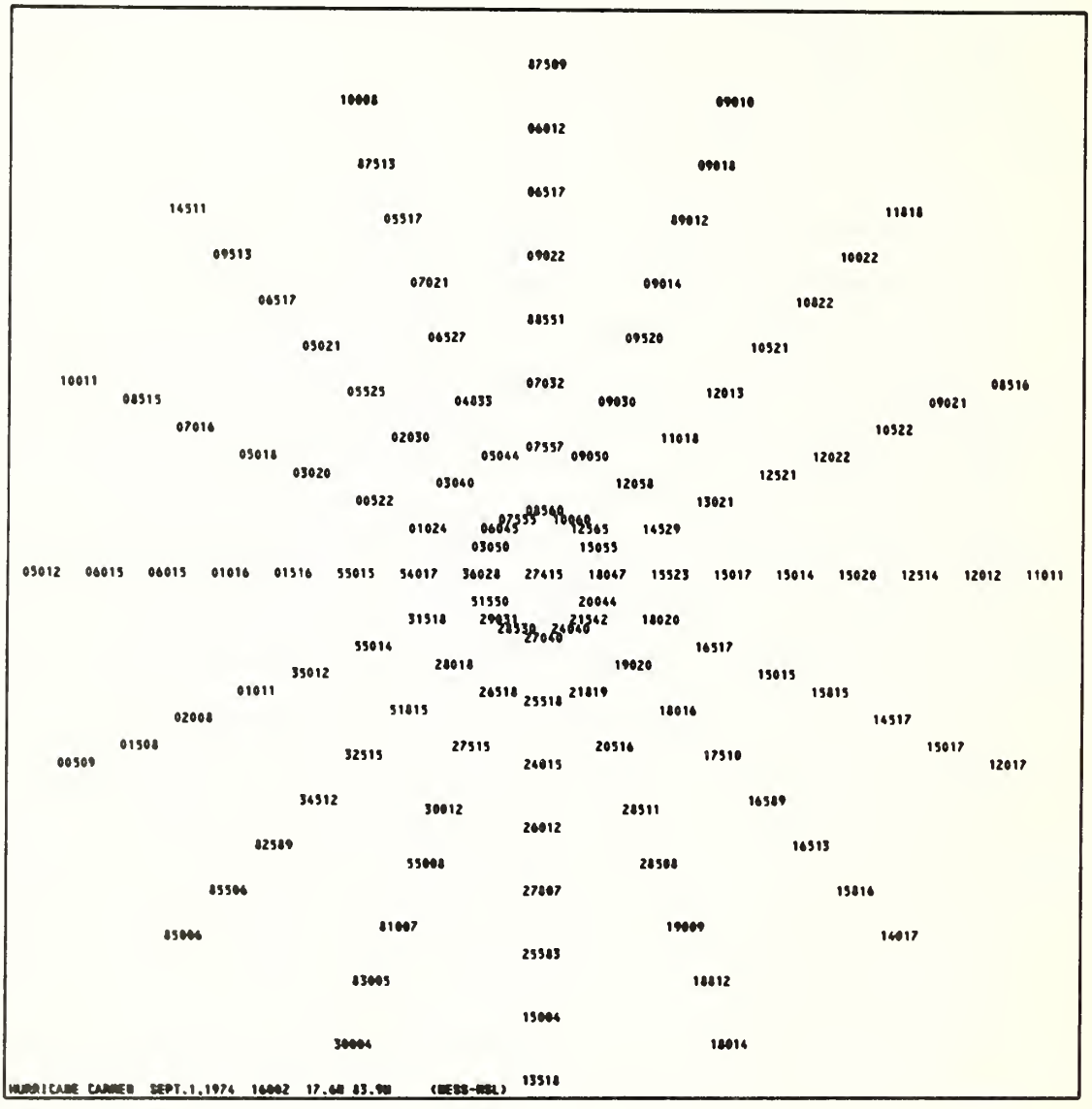

Figure 3.--Observed wind field (dddff) of hurricane Carmen, 1600 GMT, Sept. 1, 1974; windspeed in knots. The central value is the storm motion vector.

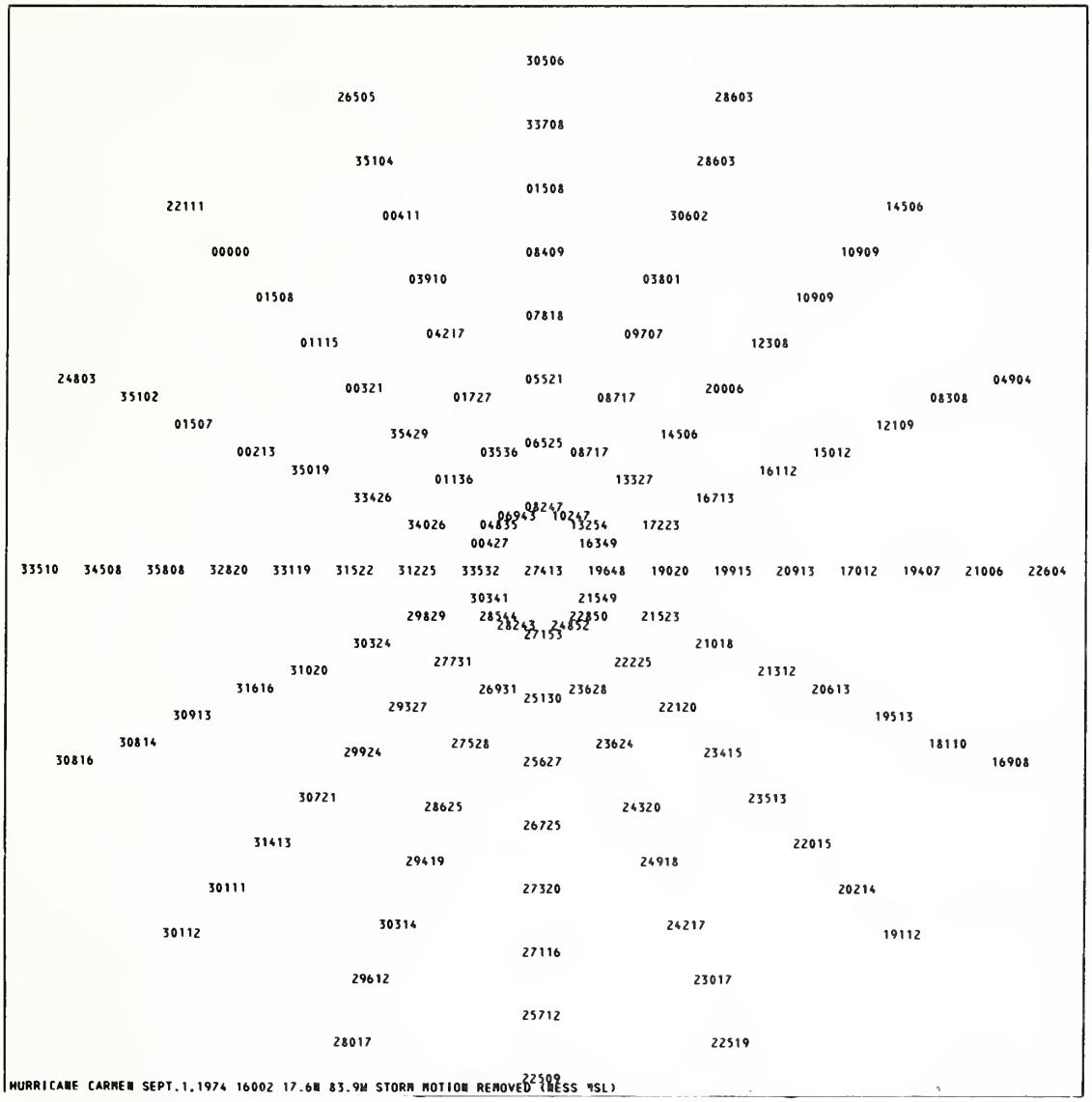

Figure 4.--Relative wind field (dddff) of hurricane Carmen, 1600 GMT, Sept. 1, 1974; windspeed in knots.

2. Measurement of Cloud Band Crossing Angle

Except for the hurricane Camille case, pictures from the visible channel (0.5 to 0.7 μm) of the Synchronous Meteorological Satellite (SMS-1) were used to determine the orientation of the low-level convective cloud bands. The resolution of the SMS-1 pictures used here was 1 n.mi. For Camille ESSA 9 data were used, with a picture resolution of 2 n.mi. which was quite adequate for determining the orientation of the cloud bands. Figure 5 is the SMS-1 picture of hurricane Carmen on Sept. 1, 1974, while figure 6 shows the orientation of the cloud bands.

Once the cloud band orientations were transferred from the gridded pictures to a Mercator map, a polar grid overlay was used to extract α_{cld} at the grid points.

Unlike a wind vector, the orientation of a cloud band can be assigned two directions, as shown in figure 7. In order to preserve inward (-) and outward (+) measurements of the crossing angles, the direction was always assigned in a cyclonic sense about the storm center. The angles were measured with respect to tangents to concentric circles centered on the storm eye. Note that the limits of α_{cld} are $\pm$ 90°. For points where no low cloud band could be seen, or the interpolated distance between cloud bands was greater than 3° latitude (180 n.mi.), or the extrapolated distance from the nearest cloud band was greater than 1° latitude (60 n.mi.), 999 was encoded to indicate that the crossing angle was missing. Values for α_{cld} were obtained at 77% of the polar grid points. Missing values were usually located at the outer radii, over land, and in clear to partly-cloudy areas.

3. Extraction of Infrared Radiation Temperature

Scanning Radiometer Infrared (SRIR) measurements of equivalent blackbody temperature (T_{BB}) obtained from polar-orbiting satellites are routinely mapped in digital form at full resolution (approx. 5 n.mi. at subpoint) and stored on magnetic tape. No SRIR data tape existed for Camille, while the data tape for Carmen on Sept. 5 contained much noise and missing data. Thus of the 10 storm cases, SRIR coverage was available for only 8. Because the infrared temperatures (radiances) were obtained by the NOAA-II polar-orbiting satellite, the measurements were made at slightly different times. However, all the measurements were made within $\pm$ 1 hour of the 1600 GMT compositing time with the exception of the Sept. 1, hurricane Carmen case in which the measurements were made at 1442 GMT. This case is shown in figure 8.

A program was devised to calculate the latitude and longitude of each grid point; T_{BB} was then extracted from the tape for these locations. To insure that the T_{BB} selected would represent a suitable area, T_{BB} was averaged over 3 x 3 scan spots, or a 15 x 15-n.mi. area for each grid point.

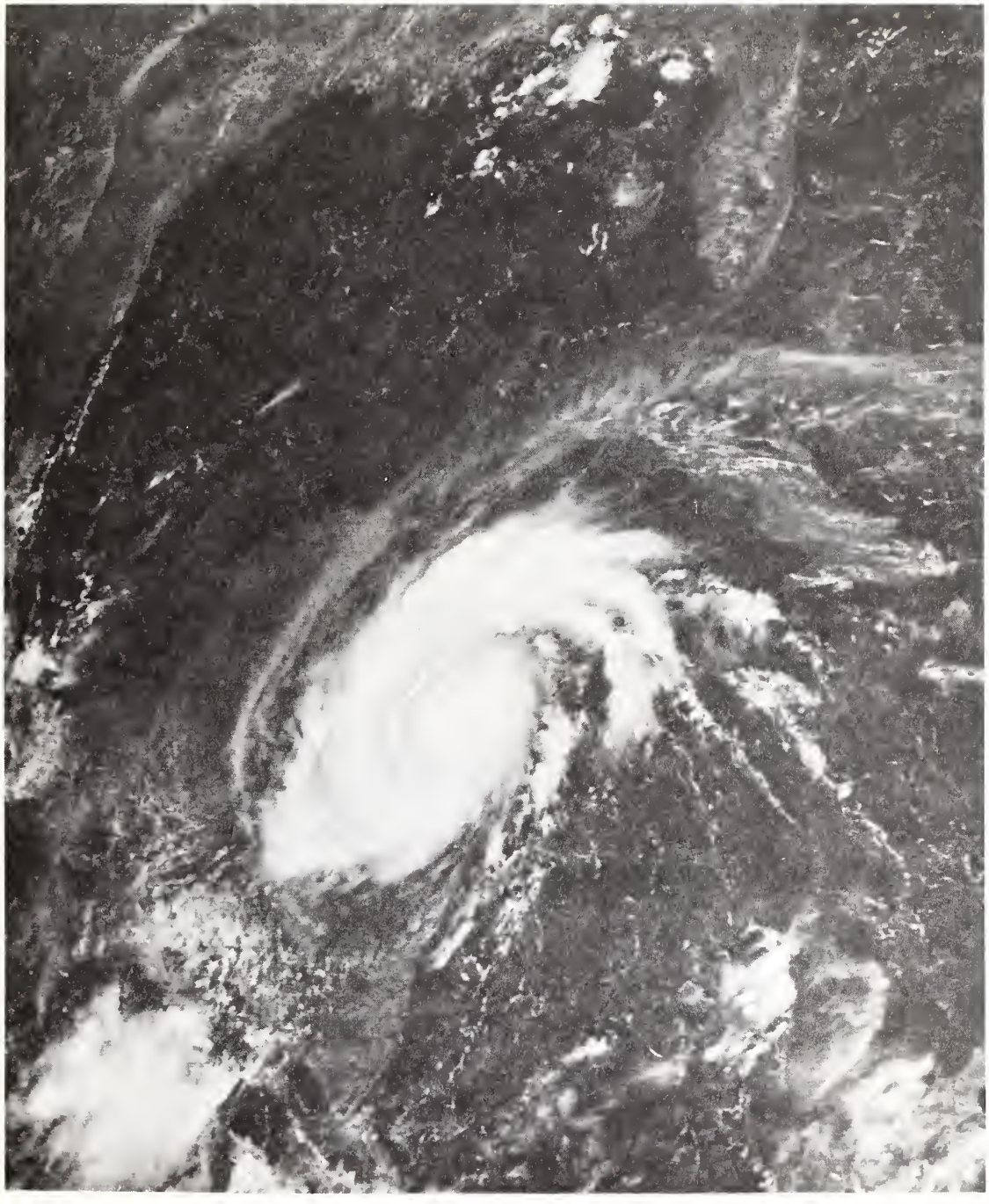

Figure 5.--SMS-1 picture of hurricane Carmen, 1600 GMT, Sept. 1, 1974. Eye position: 17.6N, 83.9W.

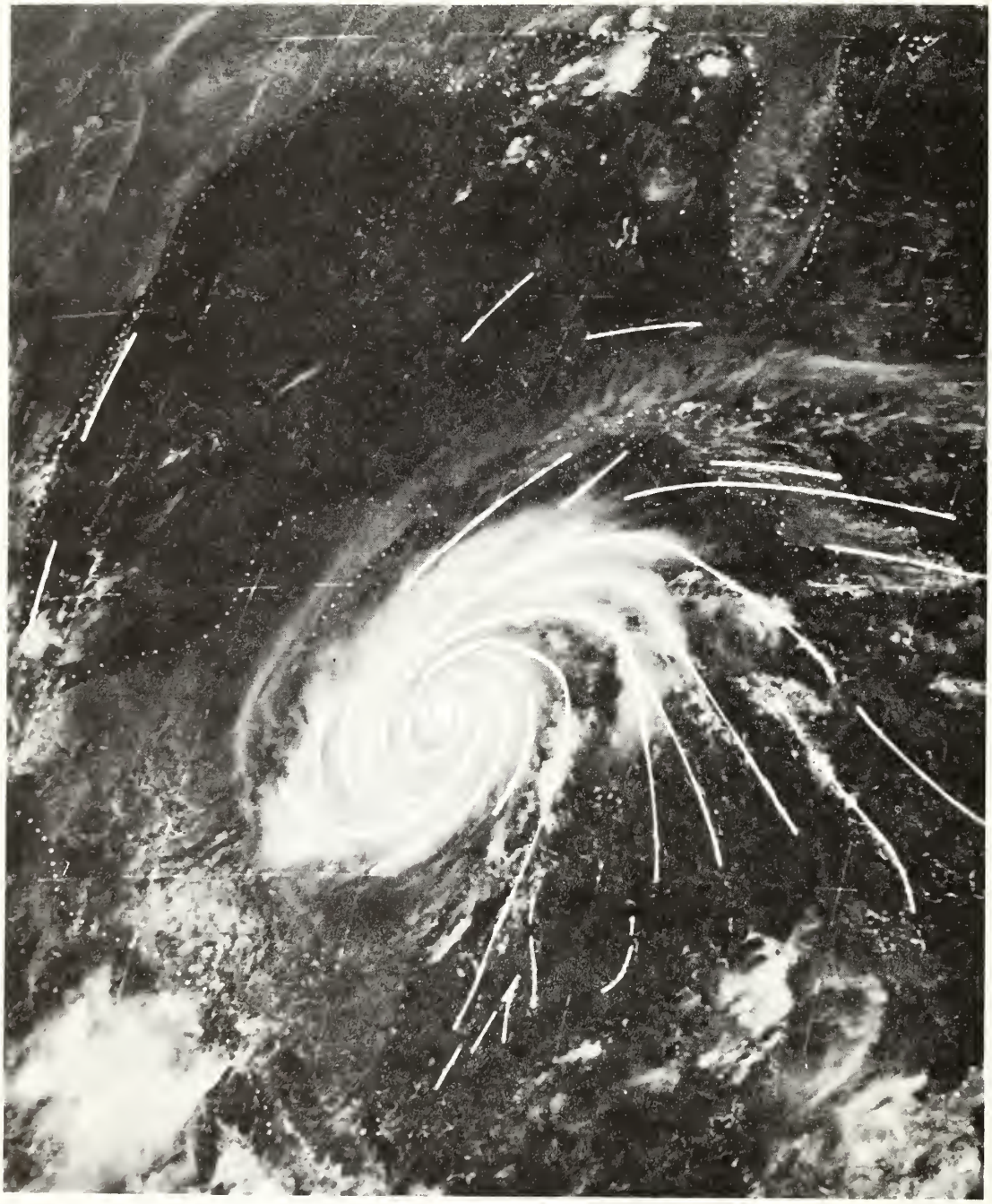

Figure 6.--SMS-1 picture of hurricane Carmen, 1600 GMT, Sept. 1, 1974 with orientations of low-level convective cloud bands used to determine the cloud band crossing angle.

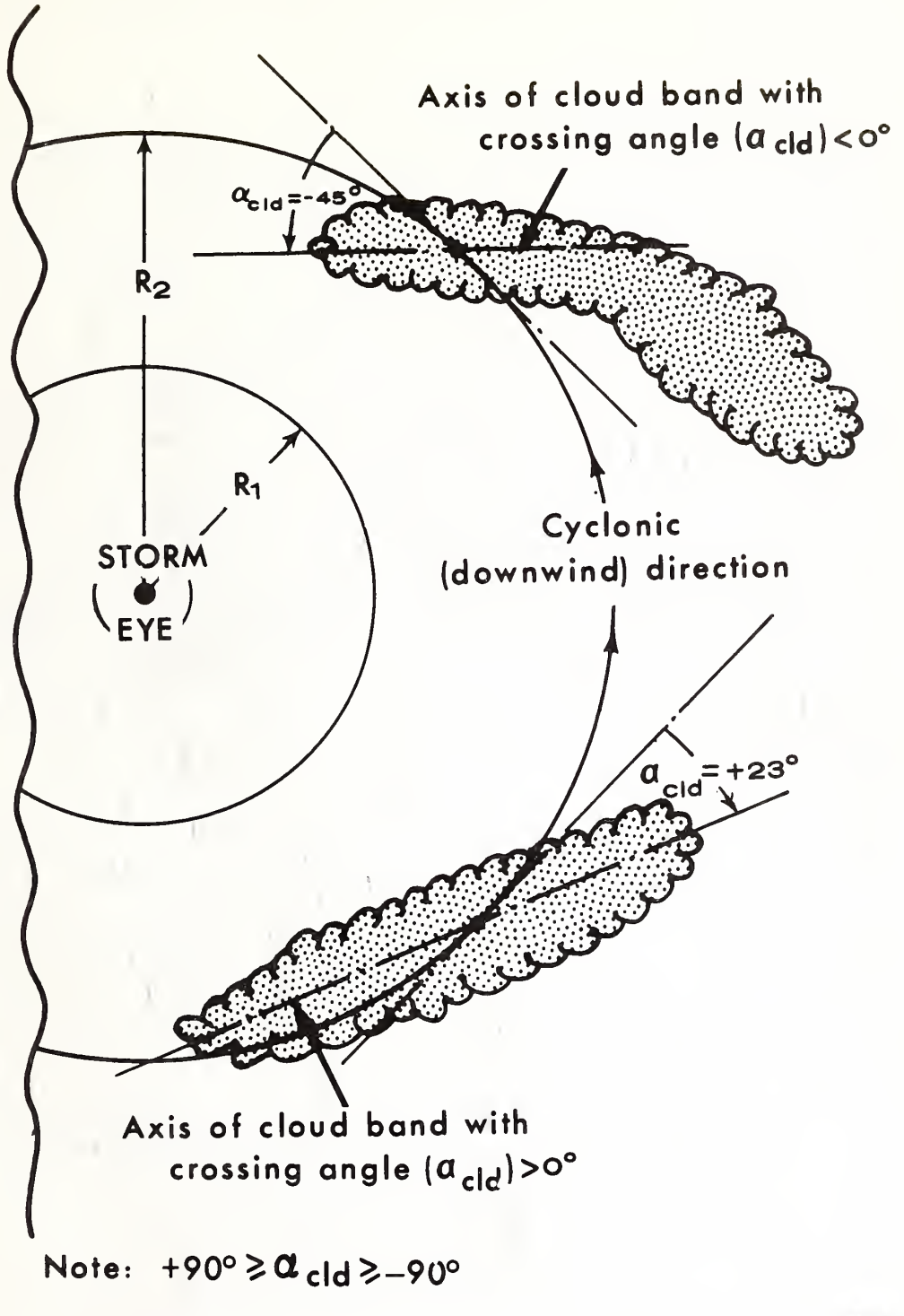

Figure 7.--Schematic showing how the cloud band crossing angles (α_{cld}) were assigned.

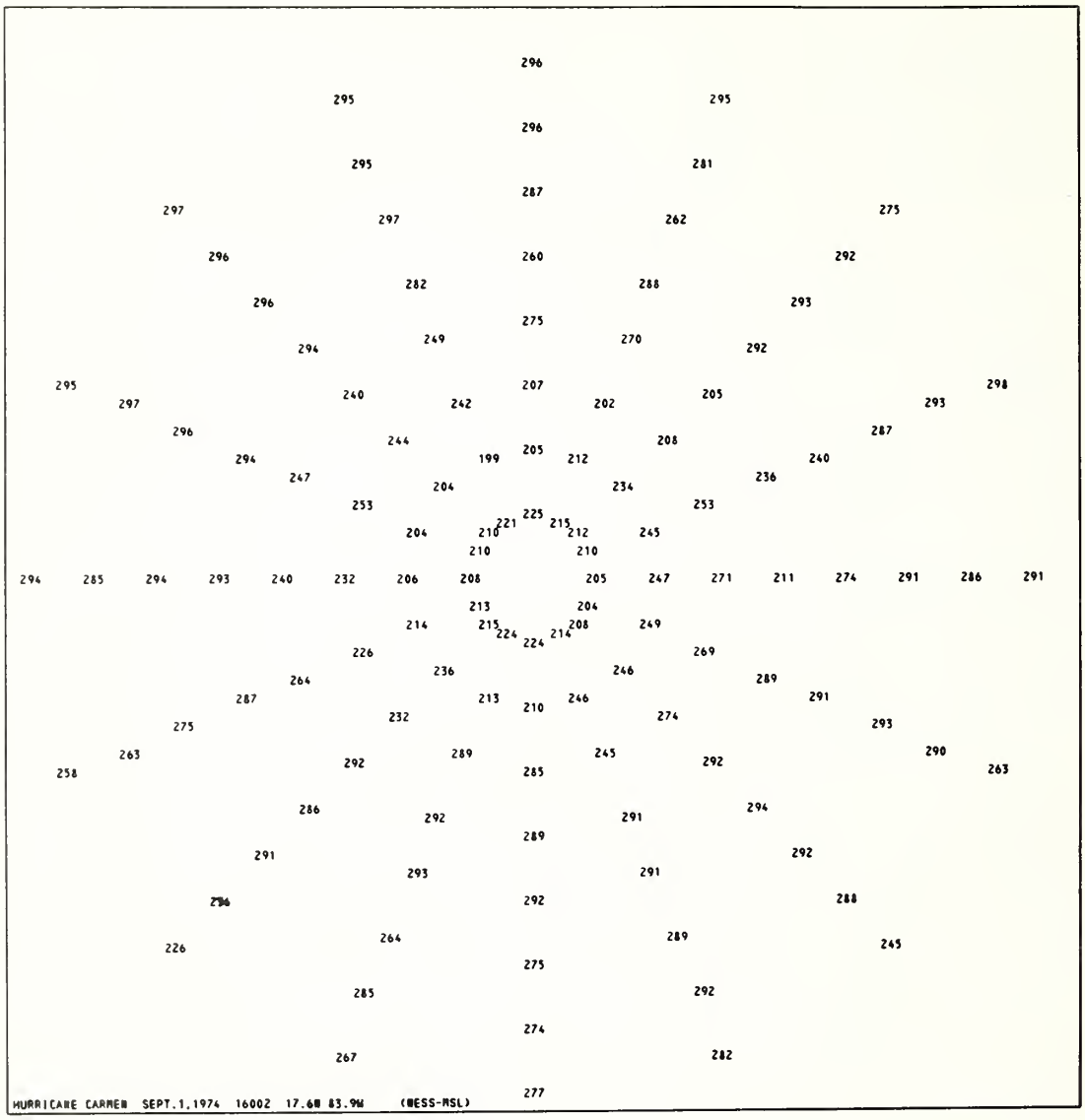

Figure 8.--NOAA II Infrared temperatures (T_{BB})°K for hurricane Carmen, 1442 GMT, Sept. 1, 1974.

Comparison with full-scale resolution data indicated that the 3 x 3 scan-spot average preserved the variations in temperature over the effective radiating surfaces, and was judged to be compatible with the scale and reliability of the windspeed data.

C. Correlation Techniques

Linear correlation and regression coefficients were calculated between the two satellite data parameters and (first) the observed windspeed (v_{obs}), and (second) the relative windspeed (v_{rel}). Correlation coefficients were calculated separately for each storm case at each radius. Radially cumulative correlations for each storm case were also calculated for radii 1° to 8°. Finally, radial and radially cumulative correlations were calculated for all the storm cases combined.

Linear correlations were also made between the observed and relative windspeeds (v_{obs}, v_{rel}) and their respective crossing angles (α_{obs}, α_{rel}).

All the linear correlations were evaluated to determine whether the parameters were related to the windspeed when the data were stratified either by storm case or by radius. Both satellite parameters were found to be related to the windspeed and to the radial distance from the storm center (R). To isolate the effectiveness of the two satellite data parameters in specifying the windspeed distribution, a Stagewise Screening Regression Method and later a Stepwise Multiple Regression Method were applied to the data. Results of the correlation and regression analysis are discussed in section III.

D. Data Accuracy and Representativeness of Cases

Mean errors were estimated to be $\pm$ 5° for α_{cld} and $\pm$ 3°C for the full resolution T_{BB}. Natural variations of the wind in time and space along with inaccuracies in wind measurement make it difficult to assign limits of accuracy to the observed wind fields. Noting the natural variations found by Gentry (1964), mean errors of $\pm$ 10° in direction and $\pm$ 20% in speed may be too small. On the other hand, it is likely that the large variability found by Gentry (ibid.) has been damped by smoothing in the isogon-isotach analyses.

In the 10 storm cases studied here, the maximum observed surface windspeed varied from 70 kt in hurricane Carmen (9/05/74) to 140 kt in hurricane Camille (8/17/69). Because all the storm cases were either in the Gulf of Mexico or the Caribbean Sea, some part of the storm was nearly always over land. However, because of the way in which the observed winds were composited, it is unlikely that land effects distorted the wind fields appreciably. Further, since α_{cld} was usually missing over land masses, this parameter was probably not significantly affected by the proximity of land.

In an attempt to isolate any nonrepresentative cases, linear correlations were first calculated by individual storm case. Although there

were marked differences between cases, no pattern of differences was detected, possibly because of the small number of cases. Accordingly, the individual cases will be discussed, but the statistical results will not be presented individually, except for the hurricane Carmen case of Sept. 1, 1974, which will be presented for illustration.

III. RESULTS

A. Linear Regression of Windspeed on Cloud Band Crossing Angle

1. Observed Windspeed vs. Cloud Band Crossing Angle

Table 2 shows the results of the linear regression of v_{obs} on algebraic values of α_{cld} for each radius (R) for the Sept. 1, 1974 hurricane Carmen case. In testing the relation involving the crossing angles, correlations were made by treating the angles first as algebraic and then as absolute values. The algebraic means of α_{cld} became more inward while the mean windspeed decreased with increasing radius in the storm. (Winds were used only if coincident with α_{cld} values.)

Table 2.--Linear regression of observed windspeed (v_{obs}) on algebraic values of the cloud band crossing angle (α_{cld}) at separate radii for hurricane Carmen, 1600 GMT, Sept. 1, 1974.

n	R (deg)	$\overline{v_{obs}}$ (kt)	$\overline{\alpha_{cld}}$ (deg)	r	a (kt)	b (kt/deg)	S (kt)
16	1	43.9	-17.81	-0.40	36.08	-0.44	10.87
16	2	25.8	-22.19	-0.38	18.00	-0.35	8.26
16	3	20.4	-26.56	-0.16	17.76	-0.10	6.56
9	4	17.8	-36.39	0.45	32.81	0.41	6.27
8	5	16.4	-42.50	0.65	30.31	0.33	4.08
8	6	15.7	-38.13	0.08	16.78	0.03	4.34
7	7	14.4	-35.71	-0.64	9.59	-0.14	2.68
4	8	13.0	-50.63	-0.77	0.14	-0.24	2.36

The correlation coefficients for individual radii should be considered only as crude estimates because the sample is so small. For a given radius, the regression equation is: $v_{obs} = a + b[\alpha_{cld}]$; the standard error about this line is given under S.

Since α_{cld} for the Sept. 1 hurricane Carmen case showed only inward cloud band crossing angles, the linear regression coefficients derived using the absolute values of α_{cld} are not shown because the results would be identical to those given in table 2. In cases where some outward $+\alpha_{cld}$ values were measured, the regression results obtained by using the absolute values would be slightly different. The correlations of v_{obs} with

α_{cld} at individual radii for the other nine cases were small and even changed sign from one case to another.

Table 3 shows the results of the radially cumulative regression, from R = 1° to 8°, of v_{obs} on the algebraic value of α_{cld} for the Sept. 1, hurricane Carmen case. The bottom row shows the results for the entire storm area.

Table 3.--Radially cumulative linear regression of observed windspeed (v_{obs}) on algebraic values of the cloud band crossing angle (α_{cld}) for hurricane Carmen, 1600 GMT, Sept. 1, 1974.

n	ΣR (deg)	$\bar{v}_{obs}$ (kt)	$\bar{\alpha}_{cld}$ (deg)	r	a (kt)	b (kt/deg)	S (kt)
16	1-1	43.9	-17.81	-0.40	36.08	-0.44	10.87
32	1-2	34.8	-20.00	-0.16	30.73	-0.20	13.69
48	1-3	30.0	-22.19	0.01	30.37	0.02	13.76
57	1-4	28.1	-24.43	0.18	33.07	0.20	13.46
65	1-5	26.6	-26.65	0.30	34.78	0.31	12.90
73	1-6	25.5	-27.91	0.33	34.51	0.32	12.52
80	1-7	24.5	-28.59	0.32	32.92	0.30	12.43
84	1-8	23.9	-29.64	0.34	32.93	0.30	12.26

Note that the correlation coefficients change sign and remain positive as the radius increases. This change in sign appeared in all but one of the storm cases. The radially cumulative regression equations for the other cases also showed that, at the higher energy radii of a storm (viz, $R \leq 2°$), larger inward (more negative) low cloud band crossing angles are associated with higher windspeed, while at $R > 2°$, smaller inward (less negative) cloud band crossing angles are associated with higher windspeed.

The results of the regression calculations for combined storm cases, by radius, are shown in tables 4 and 5. Comparison of the two tables shows the differences between the algebraic and absolute values of α_{cld}. As expected, the mean absolute values of α_{cld} were larger than the mean algebraic values; in either case, they are poorly related to the windspeed.

Table 4.--Linear regression of observed windspeed (v_{obs}) on algebraic values of the cloud band crossing angle (α_{cld}) at separate radii for 10 combined cases.

n	R (deg)	$\bar{v}_{obs}$ (kt)	$\bar{\alpha}_{cld}$ (deg)	r	a (kt)	b (kt/deg)	S (kt)
160	1	50.0	-12.84	-0.17	47.17	-0.22	13.23
156	2	34.6	-17.93	-0.10	32.94	-0.09	10.39
153	3	27.4	-21.42	0.04	27.99	0.03	8.55
137	4	23.4	-23.38	0.21	25.56	0.09	7.48
123	5	20.0	-25.53	0.10	20.82	0.03	6.26
110	6	17.6	-25.84	0.09	18.17	0.02	5.86
86	7	15.9	-27.73	0.16	16.67	0.03	5.32
64	8	14.7	-30.74	0.10	15.31	0.02	5.30

Table 5.--Linear regression of observed windspeed (v_{obs}) on absolute values of the cloud band crossing angle ($|\alpha_{cld}|$) at separate radii for 10 combined cases.

n	R (deg)	$\bar{v}_{obs}$ (kt)	$\overline{\lvert\alpha_{cld}\rvert}$ (deg)	r	a (kt)	b (kt/deg)	S (kt)
160	1	50.0	13.53	0.18	46.56	0.25	13.20
156	2	34.6	18.25	0.11	32.59	0.11	10.37
153	3	27.4	21.52	-0.03	27.92	-0.02	8.55
137	4	23.4	25.42	-0.22	26.38	-0.12	7.47
123	5	20.0	28.05	-0.25	22.65	-0.09	6.10
110	6	17.6	29.66	-0.14	18.97	-0.05	5.83
86	7	15.9	34.42	-0.16	17.08	-0.03	5.32
64	8	14.7	38.95	-0.09	15.74	-0.03	5.31

The radially cumulative regression results for the 10 combined storm cases are shown in tables 6 and 7.

When the data from all 10 cases were combined using both algebraic and absolute values of α_{cld} at separate radii (tables 4 and 5) and cumulative radii (tables 6 and 7), the correlation changed sign at $R \geq 3°$, as in the other cases. Although the correlation was quite low, the relation shown for the inner radii, (tables 2 to 7) is opposite the relation implied by eq. (10). The results for the inner radii tend to support the relation derived by Malkus and Riehl (1959). In that study, a dynamic model of a steady-state mature hurricane was evolved in which the windspeed at different radii of a storm was directly proportional to the inflow angle of

Table 6.--Radially cumulative linear regression of observed windspeed (v_{obs}) on algebraic values of the cloud band crossing angle (α_{cld}) for 10 combined cases.

n	ΣR (deg)	$\bar{v}_{obs}$ (kt)	$\bar{\alpha}_{cld}$ (deg)	r	a (kt)	b (kt/deg)	S (kt)
160	1-1	50.0	-12.84	-0.17	47.17	-0.22	13.23
316	1-2	42.4	-15.35	0.01	42.56	0.01	14.29
469	1-3	37.5	-17.33	0.13	40.32	0.16	14.39
606	1-4	34.3	-18.70	0.20	38.33	0.22	14.25
729	1-5	31.9	-19.85	0.22	36.13	0.21	14.17
839	1-6	30.0	-20.64	0.22	34.04	0.20	14.17
925	1-7	28.7	-21.30	0.22	32.34	0.17	14.17
989	1-8	27.8	-21.91	0.22	31.42	0.17	14.15

Table 7.--Radially cumulative linear regression of observed windspeed (v_{obs}) on absolute values of the cloud band crossing angle ($|\alpha_{cld}|$) for 10 combined cases.

n	R (deg)	$\bar{v}_{obs}$ (kt)	$\|\bar{\alpha}_{cld}\|$ (deg)	r	a (kt)	b (kt/deg)	S (kt)
160	1-1	50.0	13.53	0.18	46.56	0.25	13.20
316	1-2	42.4	15.86	0.00	42.37	0.00	14.29
469	1-3	37.5	17.71	-0.12	40.32	-0.16	14.40
606	1-4	34.3	19.45	-0.22	39.44	-0.26	14.17
729	1-5	31.9	20.90	-0.28	38.18	-0.30	13.95
839	1-6	30.0	22.05	-0.30	36.68	-0.30	13.85
925	1-7	28.7	23.20	-0.32	35.32	-0.29	13.77
989	1-8	27.8	24.22	-0.34	34.96	-0.30	13.65

air trajectories, while the relation shown in eq. (10) is based on inflow angles of streamlines.

The slight improvement in the correlation, when calculated for the entire area, appears to be largely due to the relation between tangential windspeed and radial distance discussed in chapter I. (See eq. 1.) The dependence of cloud band crossing angles on radial distance from the storm center will be discussed in section III.E.

2. Relative Windspeed vs. Cloud Band Crossing Angle

Relative windspeed (v_{rel}) is defined as the magnitude of the vector obtained by subtracting the storm motion vector from the observed wind vector. Coefficients of the linear regression of v_{rel} on α_{cld} are shown in tables 8, 9, 10, and 11. Comparing these tables with tables 4, 5, 6, and 7, it is seen that the relative windspeed was only slightly better correlated with the cloud band crossing angle than was the observed wind.

Table 8.--Linear regression of relative windspeed (v_{rel}) on algebraic values of the cloud band crossing angle (α_{cld}) at separate radii for 10 combined cases.

n	R (deg)	$\bar{v}_{rel}$(kt)	$\bar{\alpha}_{cld}$(deg)	r	a (kt)	b (kt/deg)	S (kt)
160	1	49.9	-12.84	-0.08	48.64	-0.10	12.36
156	2	34.5	-17.93	-0.04	34.01	-0.03	8.78
153	3	27.3	-21.42	0.14	29.41	0.10	8.19
137	4	22.7	-23.38	0.16	24.45	0.08	7.76
123	5	18.6	-25.53	0.15	20.02	0.06	7.68
110	6	16.0	-25.84	0.14	17.22	0.05	7.65
86	7	13.8	-27.73	0.18	14.93	0.04	7.44
64	8	12.8	-30.74	0.19	14.37	0.05	7.84

Table 9.--Linear regression of relative windspeed (v_{rel}) on absolute values of the cloud band crossing angle ($|\alpha_{cld}|$) at separate radii for 10 combined cases.

n	R (deg)	$\bar{v}_{rel}$(kt)	$\|\bar{\alpha}_{cld}\|$(deg)	r	a (kt)	b (kt/deg)	S (kt)
160	1	49.9	13.53	0.10	48.13	0.13	12.34
156	2	34.5	18.25	0.04	33.85	0.04	8.78
153	3	27.3	21.52	-0.14	29.49	-0.10	8.19
137	4	22.7	25.42	-0.27	26.57	-0.15	7.57
123	5	18.6	28.05	-0.29	22.44	-0.14	7.42
110	6	16.0	29.66	-0.19	18.41	-0.08	7.58
86	7	13.8	34.42	-0.06	14.42	-0.02	7.55
64	8	12.8	38.95	-0.09	14.31	-0.04	7.96

As in the observed winds case, the correlation coefficients are small, but the change in sign at radius 3° is again present. The regression

results for separate radii, shown in tables 8 and 9, reveal that the absolute values of α_{cld} were only slightly better correlated with the relative windspeed than were the algebraic values. This was also true for the observed wind. Aside from some possible significance of the change in sign between 2° and 3° radii, it appears that small inward crossing angles of the cloud bands tend to accompany higher windspeed while large crossing angles tend to accompany low windspeed. This tendency was expected, but much higher correlations were anticipated.

Tables 10 and 11 show the results of the radially cumulative linear regression between v_{rel} and α_{cld} for the combined storm cases. Table 10 shows the results obtained by using the algebraic values and table 11 the absolute values of α_{cld}.

Table 10.--Radially cumulative linear regression of relative windspeed (v_{rel}) on algebraic values of the cloud band crossing angle (α_{cld}) for 10 combined cases.

n	ΣR (deg)	$\bar{v}_{rel}$(kt)	$\bar{\alpha}_{cld}$(deg)	r	a (kt)	b (kt/deg)	S (kt)
160	1-1	49.9	-12.84	-0.08	48.64	-0.10	12.36
316	1-2	42.3	-15.35	0.08	43.82	0.10	13.19
469	1-3	37.4	-17.33	0.20	41.56	0.24	13.49
606	1-4	34.1	-18.70	0.24	38.89	0.26	13.67
729	1-5	31.5	-19.85	0.26	36.52	0.26	13.95
839	1-6	29.4	-20.64	0.26	34.27	0.23	14.21
925	1-7	28.0	-21.30	0.26	32.35	0.21	14.43
989	1-8	27.0	-21.91	0.26	31.39	0.20	14.51

Table 11.--Radially cumulative linear regression of relative windspeed (v_{rel}) on absolute values of the cloud band crossing angle ($|\alpha_{cld}|$) for 10 combined cases.

n	ΣR (deg)	$\bar{v}_{rel}$(kt)	$\|\bar{\alpha}_{cld}\|$(deg)	r	a (kt)	b (kt/deg)	S (kt)
160	1-1	49.9	13.53	0.10	48.13	0.13	12.34
316	1-2	42.3	15.86	-0.07	43.74	-0.09	13.20
469	1-3	37.4	17.71	-0.19	41.68	-0.24	13.52
606	1-4	34.1	19.45	-0.29	40.52	-0.33	13.50
729	1-5	31.5	20.90	-0.34	39.13	-0.37	13.60
839	1-6	29.4	22.05	-0.36	37.47	-0.36	13.74
925	1-7	28.0	23.20	-0.36	35.72	-0.33	13.92
989	1-8	27.0	24.22	-0.38	35.29	-0.34	13.90

The correlation coefficients for the entire data sets were 0.26 for the algebraic values and -0.38 for the absolute values. The variance of relative windspeed explained was 6.9% for the algebraic values of α_{cld} and 14.6% for the absolute values. Comparable percentages for the observed windspeed were 5.0% and 11.6%, respectively. As in the observed wind case, the increase in the correlation as more and more radii were included indicates that α_{cld} is related to v_{rel} because α_{cld} itself is related to the radial distance (R) from the storm center.

B. Linear Regression of Windspeed on Infrared Temperature (T_{BB})

1. Observed Windspeed vs. Infrared Temperature

The procedure used to test for relation between the windspeed and the cloud band crossing angle was repeated, except that infrared temperature was used in place of the cloud band crossing angle. Table 12 shows the linear regression of v_{obs} on T_{BB} at separate radii for the Sept. 1 hurricane Carmen case.

Table 12.--Linear regression of observed windspeed (v_{obs}) on infrared temperature (T_{BB}) at separate radii for hurricane Carmen, 1600 GMT, Sept. 1, 1974.

n	R (deg)	$\overline{v}_{obs}$(kt)	$\overline{T}_{BB}$(°K)	r	a (kt)	b (kt/°K)	S (kt)
16	1	43.9	213.6	0.11	0.80	0.20	11.80
16	2	25.8	223.1	-0.35	63.60	-0.17	8.38
16	3	20.4	245.8	-0.46	48.74	-0.12	5.90
16	4	16.9	261.4	-0.27	31.90	-0.06	5.96
16	5	15.3	284.4	-0.52	70.94	-0.20	4.58
16	6	13.6	286.4	0.59	-66.24	0.28	4.20
16	7	12.3	284.3	0.58	-41.01	0.19	4.06
16	8	11.4	278.4	0.07	7.81	0.01	3.91

For this case, the $\overline{T}_{BB}$ increased to a maximum at the 6° radius and then slowly decreased. The v_{obs} decreased monotonically with increasing radius. The correlations at separate radii, in this and the remaining cases, was small and negative.

The radially cumulative regression results for the Sept. 1, 1974 hurricane Carmen case are shown in table 13.

Table 13.--Radially cumulative linear regression of observed windspeed (v_{obs}) on infrared temperature (T_{BB}) for hurricane Carmen, 1600 GMT, Sept. 1, 1974.

n	ΣR (deg)	$\bar{v}_{obs}$(kt)	$\bar{T}_{BB}$(°K)	r	a (kt)	b (kt/°K)	S (kt)
16	1-1	43.9	213.6	0.11	0.80	0.20	11.80
32	1-2	34.8	218.4	-0.33	103.64	-0.32	13.07
48	1-3	30.0	227.5	-0.50	97.20	-0.30	11.92
64	1-4	26.7	236.0	-0.55	88.19	-0.26	11.31
80	1-5	24.4	245.7	-0.62	85.69	-0.25	10.33
96	1-6	22.6	252.4	-0.64	84.15	-0.24	9.87
112	1-7	21.2	257.0	-0.64	82.83	-0.24	9.63
128	1-8	20.0	259.7	-0.64	81.56	-0.24	9.43

The correlation coefficients increased as additional radii were included in the data set, as was the case for the cloud band crossing angles.

As noted earlier, infrared temperatures were available for only 8 of the 10 storm cases. Table 14 shows the regression of observed windspeed (v_{obs}) on infrared temperature (T_{BB}) at separate radii for the 8 combined storm cases.

Table 14.--Linear regression of observed windspeed (v_{obs}) on infrared temperature (T_{BB}) at separate radii for 8 combined cases.

n	R (deg)	$\bar{v}_{obs}$(kt)	$\bar{T}_{BB}$(°K)	r	a (kt)	b (kt/°K)	S (kt)
128	1	50.4	216.5	-0.23	87.58	-0.17	11.40
128	2	35.7	232.6	-0.25	62.94	-0.12	9.71
128	3	28.3	247.8	-0.18	43.52	-0.06	8.39
126	4	23.6	253.5	-0.14	32.80	-0.04	7.48
124	5	19.5	265.0	-0.18	31.04	-0.04	6.79
124	6	16.3	272.9	-0.09	22.53	-0.02	6.00
123	7	13.7	276.2	0.02	12.20	0.01	5.32
122	8	12.6	280.2	-0.01	13.71	-0.00	5.06

Small, negative values of r show that infrared temperature is poorly related to the windspeed.

Table 15 shows the radially cumulative linear regression of observed windspeed (v_{obs}) on infrared temperature (T_{BB}) for 8 combined storm cases.

Table 15.--Radially cumulative linear regression of observed windspeed (v_{obs}) on infrared temperature (T_{BB}) for 8 combined cases.

n	ΣR (deg)	$\overline{v}_{obs}$(kt)	$\overline{T}_{BB}$(°K)	r	a (kt)	b (kt/°K)	S (kt)
128	1-1	50.4	216.5	-0.23	87.58	-0.17	11.40
256	1-2	43.0	224.5	-0.40	100.96	-0.26	12.06
384	1-3	38.1	232.3	-0.48	99.97	-0.27	12.05
510	1-4	34.5	237.5	-0.49	93.50	-0.25	12.19
634	1-5	31.6	242.9	-0.53	93.08	-0.25	12.07
758	1-6	29.1	247.8	-0.56	94.25	-0.26	11.87
881	1-7	26.9	251.8	-0.59	95.32	-0.27	11.73
1003	1-8	25.2	255.2	-0.61	96.87	-0.28	11.47

For the entire data set, 37.2% of the observed windspeed variance could be explained by the infrared temperature; however, the low correlation coefficients calculated at each separate radius (table 14) indicate that, as in the case of the cloud band crossing angle, the relation clearly depends on the radial distance from the storm center.

2. Relative Windspeed vs. Infrared Temperature

To determine whether relative windspeed was better related to infrared temperature than was observed windspeed, linear regressions were again computed using relative windspeed as the dependent variable. The regressions showed, as in the observed wind case, that at individual radii the correlation was low and fluctuated in sign. When the data for all radii were combined, the correlation increased significantly. For the entire data set, the correlation was -0.595. Thus, about 35.4% of the variance of the relative windspeed, as opposed to 37.2% of the variance of the observed windspeed, could be accounted for by the infrared temperature. The 1.8% difference in the explained variance is considered insignificant.

As noted earlier in the observed wind case, the relation of infrared temperature to relative windspeed also existed primarily because the infrared temperature was related to radial distance from the storm center. The predominance of negative correlation coefficients at separate radii indicated that the expected inverse relation between the windspeed and infrared temperature exists, but is too weak to be useful. The use of infrared temperature to specify the areal windspeed distribution will be discussed further in section III. E.

C. Linear Regression of Cloud Band Crossing Angle on Wind Field Crossing Angle

1. Cloud Band Crossing Angle vs. Observed Wind Crossing Angle

The cloud band crossing angle was selected as one of the satellite data parameters because it was assumed that this angle would be well correlated with the wind crossing angle (α_{obs}), which in turn was shown in eq. (10) to be related to the tangential component of the windspeed.

How well the crossing angles are correlated indicates how close the wind direction is to the orientation of low-level cloud bands. Table 16 shows results of the linear regression of algebraic values of α_{cld} on algebraic values of the crossing angle of the wind direction (α_{obs}) at separate radii for the 10 combined storm cases.

Table 16.--Linear regression of algebraic values of the cloud band crossing angle (α_{cld}) on algebraic values of the wind field crossing angle (α_{obs}) at separate radii for 10 combined cases.

n	R (deg)	$\bar{\alpha}_{cld}$(deg)	$\bar{\alpha}_{obs}$(deg)	r	a (deg)	b	S (deg)
160	1	-12.84	- 6.46	0.00	-12.84	0.00	10.68
156	2	-17.93	- 8.57	0.19	-16.90	0.12	10.82
153	3	-21.42	-11.79	0.38	-18.94	0.21	10.79
137	4	-23.38	-18.42	0.43	-17.44	0.32	15.47
123	5	-25.53	-25.85	0.42	-18.16	0.29	18.33
110	6	-25.84	-31.07	0.38	-18.29	0.24	21.72
86	7	-27.73	-31.42	0.32	-20.59	0.23	30.38
64	8	-30.74	-29.24	0.48	-21.78	0.31	26.78

Table 17 shows the results obtained by using the absolute values of the crossing angles of both the cloud bands and the wind direction. This table shows the magnitudes of the crossing angles independent of their inward (-) or outward (+) orientation.

Table 17.--Linear regression of absolute values of the cloud band crossing angle ($|\alpha_{cld}|$) on absolute values of the wind field crossing angle ($|\alpha_{obs}|$) at separate radii for 10 combined cases.

n	R (deg)	$\|\bar{\alpha}_{cld}\|$ (deg)	$\|\bar{\alpha}_{obs}\|$ (deg)	r	a (deg)	b	S (deg)
160	1	13.53	13.47	0.08	12.59	0.70	10.65
156	2	18.25	16.01	0.16	15.68	0.16	10.88
153	3	21.52	20.04	0.34	15.38	0.31	10.94
137	4	25.42	25.20	0.30	16.84	0.34	16.35
123	5	28.05	31.97	0.26	20.66	0.23	19.47
110	6	29.66	39.94	0.24	21.24	0.21	22.80
86	7	34.42	46.99	0.12	27.97	0.14	31.83
64	8	38.95	49.91	0.28	23.01	0.32	29.41

Comparison of the algebraic means with the absolute means at each radius in tables 16 and 17 reveals the extent to which the outward-oriented crossing angles (+ values) reduced the average inward algebraic crossing angles (- values) at each radius. Table 17 shows that the mean absolute values of the crossing angle of the observed wind ($|\alpha_{obs}|$) became larger than the mean absolute values of the cloud band crossing angle ($|\alpha_{cld}|$) beyond the 4° radius. This result was anticipated since the upper limits of the cloud band crossing angles were $\pm$ 90°, while the upper limits for the observed wind crossing angles were $\pm$ 180°.

It was expected that the correlation coefficients would be higher at all radii than those shown in table 16, and that the correlations near the storm center would be higher than those found at the outer radii. Neither expectation was fulfilled. Figure 9 illustrates the ranges of, and the lack of correlation between, the crossing angle of the wind direction (α_{obs}) and the crossing angle of the low cloud bands (α_{cld}) for the 1° radius for the 10 combined storm cases. The lack of correlation can also be seen by simple inspection of figure 9.

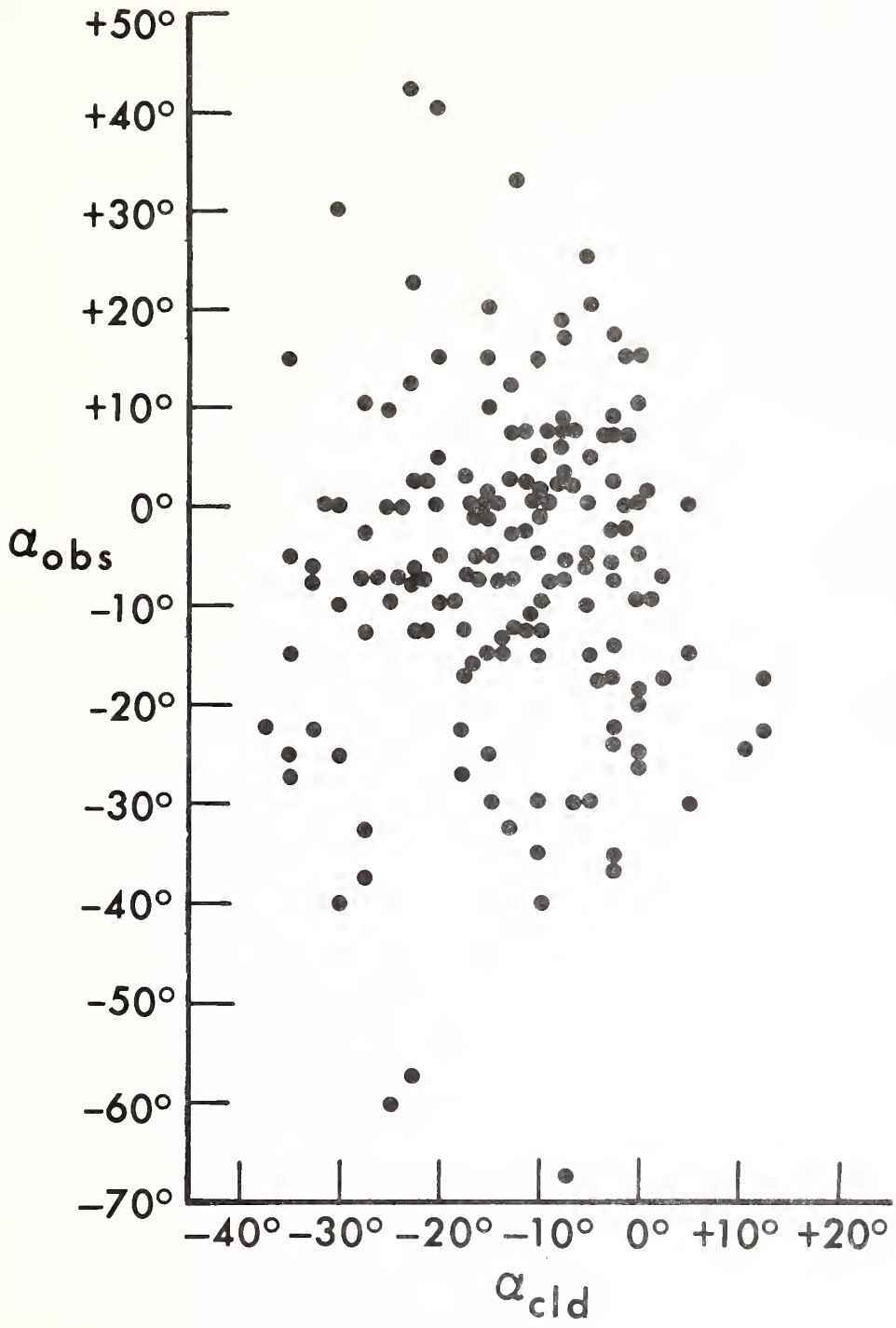

Figure 9.--Wind field crossing angle (α_{obs}) vs. cloud band crossing angle (α_{cld}) for the 1° radius for 10 combined storm cases. (N = 160).

To what extent the results presented in table 16 are representative is largely dependent upon the reliability of the wind direction. Even though a field analysis method was used to extract the wind directions and speeds, the areal gaps in the observations may have been too large, or the $\pm$ 8-hour compositing time interval may have been too long to yield an accurate wind field. Some of the poor correlation may also have been caused by differences in altitude of the winds and the cloud bands, particularly in areas with large vertical shear in the wind direction.

Because of the uncertainties in the wind fields, and the limited number of storm cases, only tentative conclusions can be drawn.

2. Cloud Band Crossing Angle vs. Relative Wind Crossing Angle

Regressions similar to those shown in tables 16 and 17 were computed using the relative wind crossing angle (α_{rel}). The correlations (not shown) of the cloud band crossing angle with the relative wind crossing angle were even lower than for the observed wind crossing angle. The highest correlation coefficient was 0.24 at the 3° radius, followed by 0.14 at 5°, and 0.13 at 4°.

D. Linear Regression of Windspeed on Wind Crossing Angle

In section III.A, it was shown that v_{obs} and α_{cld} at individual radii were poorly correlated. When all radii of the storms were combined, thereby introducing the relation of v_{obs} to R, the correlation was still only about 0.4. Further, since in section III.C, it was shown that the correlation between α_{cld} and α_{obs} at all radii was below 0.5, the question arose as to whether α_{obs} itself was related to the windspeed. Accordingly, the linear regression of v_{obs} on α_{obs} was examined. Similar computations were also made for the relative wind field.

At separate radii neither α_{obs} nor α_{rel} showed significant improvement over α_{cld} in their correlation to the windspeed. Cumulatively for all radii, the algebraic values of α_{obs} and α_{rel} showed a correlation of only about 0.1 to the windspeed while the absolute values of α_{obs} showed a correlation of about 0.4 with windspeed. Comparative values for the cloud band crossing angle were 0.25 for algebraic values and 0.36 for absolute values. Overall, the windspeed was slightly better correlated with α_{cld} than α_{obs}. This also was unexpected.

E. Screening Regression

1. Procedure

The radially cumulative correlation coefficients presented earlier increased monotonically as data from additional radii were included. Apparently, the correlation of these two satellite parameters with windspeed is related to the radial distance from the storm center, as shown by eq. (1).

To evaluate the radial relation and the effectiveness of the two satellite data parameters in specifying the windspeed distribution, a Stagewise Screening Regression Method* was applied to the data. Only selected results of this analysis will be presented.

Later in the study, a more rigorous statistical analysis, the Stepwise Multiple Regression Method,* was applied to the same data. The results obtained by this method showed only minor differences from those obtained earlier with the Stagewise Screening Method, thereby corroborating the results of the Stagewise Screening Method. In both Screening Regression Methods, any number of variables can be entered as predictors. Further, nonlinear operations can be performed on any of the variables before the regression process has begun.

In applying screening regression methods, the windspeed was usually designated as the dependent variable. However, separate runs with the Stagewise Screening Method were made by using first the radial and then the tangential variation of the windspeed as the dependent variable. The principal independent variables tested were: the radius (R), the cloud band crossing angle (α), the infrared temperature (T_{BB}), and the radial and tangential variation of α and T_{BB}. The 9 forms of the variables are shown later in column 7 of table 18.

2. Screening Regression of Observed Windspeed on Nine Independent Variables

Because coincident values of each of the variables are required for each grid point, the sample was reduced significantly. A further reduction of the sample occurred because spatial differences of the variables, which require simultaneous data at two points, were also used as variables.

For the variables screened by both methods, as shown in table 18, the absences of 1 or more of the 9 independent variables reduced the sample from a maximum possible 1120 to 601. Because 2 additional samples had been retained in the Stepwise method, the sample size then was 603.

The left side of table 18 shows the results of the Stagewise Screening Method. Only the first 10 passes through the data are shown since the variance explained by additional passes would be negligible. Under the Stepwise Multiple Regression, the step numbers show the order of selection followed by the 9 forms of the independent variables screened.

---

*See appendix for a description of screening regression methods.

Table 18.--Results of both the Stagewise Screening and the Stepwise Multiple Regressions of the observed windspeed (dependent variable) on 9 independent variables for all 10 storm cases.

Stagewise Screening Regression N = 601					Stepwise Multiple Regression N = 603				
Pass no.	Variable	Indiv. Cor. Coef.	Var. Expl. %	Δ%	Step no.	Variable	Cum. Cor. Coef.	Var. Expl. %	Δ%
1*	$R^{-0.5}$	.7932	62.9	0.4	1	$R^{-0.5}$	.7912	62.61	0.59
2	$\Delta\alpha/\Delta R$	.0988	63.3	0.4	2	T_{BB}	.7950	63.20	0.47
3+	T_{BB}	-.1080	63.7	0.3	3	$\Delta\alpha/\Delta R$	.7979	63.67	0.36
4	$\Delta T_{BB}/\Delta R$	-.0835	64.0	0.2	4	$\Delta T_{BB}/\Delta\Theta$	.8002	64.03	0.27
5	$\Delta\alpha/\Delta\Theta$	.0774	64.2	0.1	5	$\Delta\alpha/\Delta\Theta$	.8019	64.30	0.23
6**	$R^{-0.5}$	-.0418	64.3	0.1	6	α	.8033	64.53	0.23
7++	T_{BB}	-.0646	64.4	0.1	7	$\Delta T_{BB}/\Delta R$	.8048	64.76	0.06
8	$\Delta T_{BB}/\Delta\Theta$	-.0582	64.5	0.1	8	R	.8051	64.82	0.05
9	α	.0430	64.6	0.1	9	$\lvert\alpha\rvert$	.8054	64.87	
10***	$R^{-0.5}$	-.0554							

For the Stagewise Screening method, where alternating selection of the same variable is permitted, $R^{-0.5}$ was selected on the first, sixth, and tenth passes, T_{BB} was selected on the third and seventh passes, while the absolute value of the cloud band crossing angle ($|\alpha|$) and the linear radius (R) were never selected.

Both the Stepwise and Stagewise methods show correlation coefficients of 0.79, i.e., 63% of the variance of the windspeed could be explained by the radius. The first pass/step of the two methods is mathematically identical, but in subsequent passes the procedures differ (see appendix). However, both methods selected either the infrared temperature (T_{BB}) or the radial variation of the cloud band crossing angle ($\Delta\alpha/\Delta R$) as the second and third variables in order of their relation to the windspeed. Note that the correlation coefficients are given individually in the Stagewise but cumulatively in the Stepwise Method.

By either method, only about 2% additional variance of the windspeed can be accounted for by T_{BB} and α, above the 63% already accounted for by $R^{-0.5}$. The regression equations derived for each method are shown in table 18a.

Table 18a.--Screening Regression Equations derived for the observed windspeed (v_{obs}) and the 9 independent variables shown in table 18, using Stagewise and Stepwise methods.

Stagewise equation: $v_{obs} = 12.27 + 51.01[R^{-0.5}] + .09[\Delta\alpha/\Delta R] - .05[T_{BB}]$

$- .03[\Delta T_{BB}/\Delta R] + .04[\Delta\alpha/\Delta\theta] - .03[\Delta T_{BB}/\Delta\theta] + .02[\alpha]$

Stepwise equation: $v_{obs} = 27.12 + 42.85[R^{-0.5}] - .08[T_{BB}] + .09[\Delta\alpha/\Delta R]$

$- .04[\Delta T_{BB}/\Delta R] + .08[\Delta\alpha/\Delta\theta] + .08[\alpha] - .04[\Delta T_{BB}/\Delta R] - .60[R] + .04[|\alpha|]$

These equations represent the best fit between the windspeed and the nine independent variables screened. The coefficients indicate the relative importance of each variable only when the proper units are applied. The radial increments (ΔR) and the tangential increments ($\Delta\theta$) were treated as unit values since they were always taken as 1° latitude in the radial direction and 22.5° ($\pi/8$ radians) in the tangential direction.

3. Individual Correlations between Windspeed and Nine Independent Variables

Because only the variable with the highest correlation was shown in the first pass of the screening methods, the individual correlations of the remaining variables are not shown in table 18. Table 19 shows the individual relations between the windspeed and each of the nine independent variables. It is instructive to evaluate these correlation coefficients (keeping in mind that they are not statistically independent) to see which variables, or forms of the variables, are most closely related to the windspeed.

Table 19.--Correlation (r) between the windspeed (v) and the 9 independent variables shown in table 18. (N = 601).

No.	Variable	r	No.	Variable	r	No.	Variable	r
1	$R^{-0.5}$	.7932	4	$\|\alpha\|$	-.3523	7	$T_{BB}/\Delta\theta$	-.0594
2	R	-.7473	5	α	.2461	8	$\Delta\alpha/\Delta\theta$	.0203
3	T_{BB}	-.5383	6	$\Delta T_{BB}/\Delta R$	.0934	9	$\Delta\alpha/\Delta R$	-.0071

In table 19, the correlation coefficients of the nine independent variables are listed in decreasing order of importance. The subscripts "cld" and "obs" have been omitted for convenience. Both forms of the radius (R) were reasonably well correlated with the windspeed. However, the radial and tangential variations of T_{BB} and α_{cld} rank at the bottom with correlation coefficients less than 0.1.

Because eq. (10) suggested the cloud band crossing angle as one of the satellite data parameters, a combined form of the variable, $[\text{Cos } \alpha_{cld}/R]^{0.5}$ was selected for screening. Table 20 shows the first pass of the Stagewise Screening Regression run that included this variable.

Table 20.--Correlation (r) between the windspeed (v) and the 9 independent variables listed below. (N = 717).

No.	Variable	r	No.	Variable	r	No.	Variable	r
1	$R^{-0.5}$	.8021	4	T_{BB}	-.5553	7	$(\text{Cos } \alpha)^{0.5}$	.3299
2	$(\text{Cos}\alpha/R)^{-0.5}$	.7929	5	Cos α	.3428	8	α	.2325
3	R	-.7539	6	$\lvert\alpha\rvert$	-.3365	9	Θ	-.2243

In table 20, the variables are listed in decreasing order of their relation to windspeed. Note that the variable $R^{-0.5}$ is again best correlated to the windspeed, with the combined form a close second. The combined form of the variable showed no improvement over $R^{-0.5}$ itself.

Because the storm cases in this study were of different intensities, the differences in windspeed might have affected the relations. In an attempt to isolate such a bias, as well as to test whether the variation of the windspeed in the radial or tangential directions was related to the other variables, the radial ($\Delta v/\Delta R$) and tangential ($\Delta v/\Delta\Theta$) variations of the windspeed were considered separately as the dependent variable.

4. Individual Correlations between Spatial Variations of the Windspeed and Nine Independent Variables

Tables 21 and 22 show the correlation between spatial variations of the windspeed and the 9 variables shown in table 18. The coefficients in table 21 show the importance of the independent variables in decreasing order. $R^{-0.5}$ was best related to $\Delta v/\Delta R$; while again, the spatial variations rank at the bottom of the list.

Table 21.--Correlation (r) between the radial variation of the windspeed ($\Delta v/\Delta R$) and the 9 independent variables shown in table 18. (N = 601).

No.	Variable	r	No.	Variable	r	No.	Variable	r
1	$R^{-0.5}$	-.6495	4	$\|\alpha\|$	.2448	7	$\Delta\alpha/\Delta R$	.0628
2	R	.5788	5	α	-.1563	8	$\Delta T_{BB}/\Delta\Theta$	.0436
3	T_{BB}	.4232	6	$\Delta T_{BB}/\Delta R$	-.0892	9	$\Delta\alpha/\Delta\Theta$	-.0340

The results of table 21 show only the first pass of the Stagewise Screening Regression. However, when 10 passes were made through the data with ($\Delta v/\Delta R$) as the dependent variable, the variance of the radial variation of the windspeed is reduced by only 43.2%, compared with 64.7% shown in table 18. Based on the results here, the radial variations of the windspeed show a lower correlation on six of the nine variables when compared to those obtained for the windspeed itself.

Table 22 gives the results of the first pass of the Stagewise Screening Regression in which the tangential variation of the windspeed was used as the dependent variable.

Table 22.--Correlation (r) between the tangential variation of the windspeed ($\Delta v/\Delta\Theta$) and the 9 independent variables shown in table 18. (N = 601).

No.	Variable	r	No.	Variable	r	No.	Variable	r
1	α	-.1300	4	$R^{-0.5}$	-.0435	7	$\Delta T_{BB}/\Delta\Theta$	.0185
2	$\Delta\alpha/\Delta R$	-.1061	5	R	.0358	8	$\Delta\alpha/\Delta\Theta$	.0114
3	$\|\alpha\|$	.1021	6	T_{BB}	.0260	9	$\Delta T_{BB}/\Delta R$	-.0050

In table 22, all 9 independent variables show a poor relation to the tangential variation of windspeed; however, $R^{-0.5}$ has now been replaced by cloud band crossing angle (α).

After 10 screening passes, 3.7% reduction in variance of $\Delta v/\Delta\Theta$ was attained (result not shown). This small amount of explained variance in the windspeed is far below what might be considered operationally useful; however, 3.3%, or nearly all the explained variance, was accounted for by the variables α and $\Delta\alpha/\Delta R$. The negative signs of the correlation coefficients for these variables were expected from dynamical considerations. Since α was designated negative when inward (implying confluence), the negative correlation coefficient for α indicates that, in the downstream counterclockwise direction interval $\Delta\Theta$, Δv would be higher if the crossing angles were more inward. Conversely, if the crossing angles were outward (implying difluence), the windspeed would decrease downstream. Similar changes of $\Delta v/\Delta\Theta$ are indicated by evaluating the confluence/difluence implied by the sign of $\Delta\alpha/\Delta R$.

Finally, it was found that the radial variation of v_{obs} was not as closely related to the independent variables as was the windspeed itself. Thus, any bias that might have been introduced by combining storms of different intensities was not detected.

From the results of the Screening Regression, about 63% of the variance of the windspeed can be explained by $R^{-0.5}$. An additional 2% to 3% of the variance of the windspeed in the radial direction can be accounted for by the various forms of T_{BB} and α_{cld}, and as much as 3% of the variance in the tangential direction can be accounted for by α_{cld} and its radial variation.

IV. SUMMARY

Ten storm cases were studied to determine whether the areal windspeed distribution could be estimated with the use of two satellite data parameters, the cloud band crossing angle (α_{cld}) and the infrared temperature (T_{BB}). The correlations of these parameters with windspeed over the entire storm area were approximately 0.4 for α_{cld} and -0.6 for T_{BB}. However, these two parameters were found to be related to the radial distance from the storm center, R; and since it was known from earlier studies that the tangential component of the windspeed can be approximated by $R^{-0.5}$, the two parameters would be useful only to the extent that they are statistically independent of R.

When linear correlations of windspeed with the satellite data parameters were calculated for each storm case for individual radii, the correlation coefficients were low, unstable, and even changed sign from radius to radius. Further, for all 10 storm cases combined, both the algebraic and absolute values of α_{cld} were poorly correlated with both the observed (v_{obs}) and relative (v_{rel}) windspeed at separate radii. Most of the correlation coefficients were below 0.2. The correlations between T_{BB} and v_{obs} and

v_{rel} at separate radii were also smaller than 0.2, (See table 14.). Beyond the 2° radius, the signs of the coefficients were as expected (See section II.A), i.e., the correlations between the windspeed and the algebraic value of α_{cld} were mostly positive (e.g., table 4). The positive coefficients result because the windspeed decreased as α_{cld} became more inward (more negative). The only exception occurred at the innermost radii (R = 1° and 2°) where the coefficients were negative.

Relative windspeed was only slightly better correlated with α_{cld} than was the observed windspeed. Further, the absolute value of α_{cld} was only slightly better related to the windspeed than was the algebraic value. Overall, there was a tendency for a better correlation between the windspeed and α_{cld} at intermediate radii (viz, 3°, 4°, and 5°). However, most of the correlations at separate radii were less than 0.2. The correlation between T_{BB} and windspeed was better at the inner radii of the storm (viz, $R \leq 5°$).

The assumption that the orientation of the cloud bands would be closely correlated with wind direction was tested by examining the relation of α_{cld} to α_{obs} and α_{rel}. The highest correlations were generally found at $R \geq 3°$, where the correlation coefficients at separate radii were about 0.4 for α_{obs} and 0.2 for α_{rel}. Errors in the wind direction may have contributed to the poor correlations.

The α_{obs} and α_{rel} were also correlated with windspeed, the coefficients being less than 0.2. The windspeed had a slightly better correlation with α_{cld} than with α_{obs}.

Results from the Multiple Screening Regression Method showed that about 63% of the variance of the windspeed could be accounted for by the $R^{-0.5}$. Only an additional 2% to 3% could be accounted for by the various forms of T_{BB} and α_{cld}, which is not considered significant.

When nine forms of the independent variables were screened against the variation of windspeed in the tangential direction, only about 3% of the variance of $\Delta V/\Delta\Theta$ was accounted for by α_{cld} and $\Delta\alpha/\Delta R$.

V. SUGGESTIONS FOR FUTURE RESEARCH

Further exploration of the relation R^X, such as that studied by Arnold (1972), may be useful. In the absence of wind observations, a simple form of the radial relation could be used as a first guess of the windspeed distribution.

Eq. (10) relates the tangential component of the windspeed to the radius and to the wind direction crossing angle, and should therefore be tested using only the tangential component.

Changes of the windspeed in time may be better related to the two satellite parameters than is the windspeed itself. This is supported by recent unpublished work of Ushijima (1975) in which he argues that the

divergence field is one of the most important factors in the formation of the rainbands. Because the windspeed profiles in the radial direction can be generally expressed by $vR^{0.6}$ = constant, the radar-observed rainband crossing angles should become smaller when acted upon by such a profile. Based on these arguments, the 1- to 24-hour changes of the windspeed should be examined.

There are numerous ways in which satellite data can be studied with regard to the windspeed distribution problem. Short-term changes of the windspeed derived from cloud motion beyond the central dense overcast area of tropical cyclones can be obtained from SMS data and should be used along with conventional data. It has been suggested by Gruber (1975) that the perturbation of the infrared temperature at individual radii be tested for possible relation to the asymmetries of the windspeed. Other forms of the infrared temperature field could also be studied.

Finally, studies similar to those of Gentry (1964) and Senn and Hiser (1959), but with accompanying satellite data, are needed to shed more light on relations between the low-level convective cloud bands or radar-observed rainbands and the windspeed in tropical cyclones.

VI. ACKNOWLEDGEMENTS

I wish to thank Professor Anandu D. Vernekar for his interest and encouragement and L. F. Hubert for suggesting the study and for his valuable consultation. Thomas I. Babicki provided extensive programming support; Charles L. Earnest, a program to extract infrared temperatures; Dr. C. M. Hayden, L. D. Herman, and F. W. Nagle assisted with the screening regression programs; Leonard D. Hatton, drafting; Gene A. Dunlap, photography; Helen M. Hamlett, typing; Gerald A. Delaney, AG1 of the Fleet Weather Central, Suitland, collection of the Hurricane reconnaissance data; R. Nilsestuen, revising and editing. The Manpower Utilization Committee made this paper possible via a NOAA scholarship.

VII. SELECTED BIBLIOGRAPHY

Arnold, C. P., Jr., Capt., 1972: Wind Speed Envelope Model of Tropical Cyclones. Air Weather Service Technique Development Summary, Jun-Aug., pp. 1-2.

Ausman, M., 1959: Some Computations of the Inflow Angles in Hurricanes near the Ocean Surface. Report on Research Prepared under Contract No. N6ori-0236, Project NR 082-120, Office of Naval Research, 19 pp.

Brand, S., and J. W. Blelloch, 1975: Cost Effectiveness of Typhoon Forecast Improvements. Bulletin of the American Meteorological Society, Vol. 56, No. 3, pp. 352-361.

Byers, H. R., 1944: General Meteorology. New York, McGraw-Hill Book Company, Inc., pp. 434-436.

Dvorak, V. F., 1973: A Technique for the Analysis and Forecasting of Tropical Cyclone Intensities from Satellite Pictures. NOAA Technical Memorandum NESS 45, 19 pp.

Frank, N., 1974: Personal Communication.

Fritz, S., L. F. Hubert, and A. Timchalk, 1966: Some Inferences from Satellite Pictures of Tropical Disturbances. Monthly Weather Review, Vol. 94, No. 4, pp. 231-236.

Gentry, C. R., 1964: A Study of Hurricane Rainbands. National Hurricane Research Project Report No. 69, 85 pp.

Gruber, A., 1975: Personal Communication.

Haurwitz, B., 1935: The Height of Tropical Cyclones and of the "Eye" of the Storm. Monthly Weather Review, Vol. 63, No. 2, pp. 45-49.

Hawkins, H. F., 1962: Vertical Wind Profiles in Hurricanes. National Hurricane Research Project Report No. 55, 16 pp.

Hubert, L. F., A. Timchalk, and S. Fritz, 1969: Estimating Maximum Wind Speed of Tropical Storms from High Resolution Infrared Data. ESSA Technical Report NESC 50, 33 pp.

Hughes, L. A., 1952: On the Low-Level Wind Structure of Tropical Storms. Journal of Meteorology, Vol. 9, No. 6, pp. 422-428.

Jelesnianski, C. P., 1966: Numerical Computations of Storm Surges Without Bottom Stress. Monthly Weather Review, Vol. 94, No. 6, pp. 379-394.

Jordan, E. S., 1952: An Observational Study of the Upper Wind Circulation Around Tropical Storms. Journal of Meteorology, Vol. 9, No. 5, pp. 340-346.

Malkus, J. S. and H. Riehl, 1959: On the Dynamics and Energy Transformations in Steady-State Hurricanes. National Hurricane Research Project No. 31, 31 pp.

Miller, B. I., 1958: The Three-Dimensional Wind Structure Around a Tropical Cyclone. National Hurricane Research Project Report No. 15, 41 pp.

Riehl, H., 1954: Tropical Meteorology. New York and London, McGraw-Hill Book Company, Inc., pp. 300-307.

_____, 1963: Some Relations Between Wind and Thermal Structure of Steady State Hurricanes. Journal of the Atmospheric Sciences, Vol. 20, pp. 276-287.

Schacht, E. J., 1946: A Mean Hurricane Sounding for the Caribbean Area. Bulletin of the American Meteorological Society, Vol. 27, No. 6, pp. 324-327.

Senn, H. V., and H. W. Hiser, 1959: On the Origin of Hurricane Spiral Rainbands. Journal of Meteorology, Vol. 16, No. 4, pp. 419-426.

Shea, D. J., and W. M. Gray, 1972: The Structure and Dynamics of the Hurricanes Inner Core Region. Atmospheric Science Paper No. 182, Dept. of Atmospheric Science, Colorado State University, Fort Collins, Colorado, 134 pp.

Sheets, R. C., and P. Grieman, 1975: An Evaluation of the Accuracy of Tropical Cyclone Intensities and Locations Determined from Satellite Pictures. NOAA Technical Memorandum ERL WMPO-20, 36 pp.

Timchalk, A., L. F. Hubert, and S. Fritz, 1965: Wind Speeds from Tiros Pictures of Storms in the Tropics. Meteorological Satellite Laboratory Report No. 33, U. S. Dept. of Commerce, Washington, D. C., 33 pp.

Ushijima, T., 1975: Origin and Behavior of Rain Bands in Tropical Cyclones. To be published, Japan Meteorological Agency.

VIII. APPENDIX

DESCRIPTION OF SCREENING REGRESSION METHODS

Screening Regression methods are useful techniques in isolating from a set the important or significant independent variables that can be used as predictors. In this study, first a Stagewise Screening Regression Method[1] was utilized (Courtesy: F. W. Nagle, NESS); subsequently, a Stepwise Multiple Regression Method[2] was applied (Courtesy: C. M. Hayden, NESS).

The first step of both methods is to calculate the individual simple linear correlation coefficients (r_{1n}) between the dependent variable X_1 and each of the independent variables $X_2, X_3, \ldots, X_n$. The variable X_k is first selected such that $r_{1k}^2 > r_{1i}^2$; from this point, the two procedures differ.

In the Stagewise method, the error ($E_{1.k}$) about the regression line $\hat{X}_1 = b_{1k}X_k$ is then treated as the dependent variable with the foregoing process repeated until there is no significant reduction in the explained variance of the dependent variable ($E_{1.i}$).

In the Stepwise Multiple Regression method, once the largest r_{1k}^2 has been selected, the partial correlation coefficients, $r_{1i.k}$ for $i,k = 2.....n$ and $i \neq k$ are calculated. The variable X_g is then selected such that $r_{1g.k}^2 > r_{1i.k}^2$ where $g,k = 2.....n$ and $g \neq i,k$. The process of selecting the variable with the highest partial correlation coefficient is continued until an "F test" shows no significance or all of the independent variables have been selected.

Although the Stagewise method allows for a repetitive selection of the same independent variable on alternating passes, while the Stepwise Multiple Regression process allows for the selection of each independent variable only once, the results obtained by applying both methods were very similar. Certainly, the Stagewise method is a logical procedure, but because it operates directly on the residual error ($E_{1.k}$) after the first pass, it is not a statistically rigorous method, as is the Stepwise Multiple method, which operates directly on the variance explained by each of the independent variables.

[1]Unpublished Program, CARP, NESS, World Weather Bldg., Washington, D. C.

[2]Biomedical Computer Program, BMD02R, University of California, Los Angles, Jan. 1964, Revised Sept. 1965, W. J. Dixon, Editor.

*U.S. GOVERNMENT PRINTING OFFICE: 1976 210-801/416 1-3

(Continued from inside front cover)

NESC 54 Estimating Cloud Amount and Height From Satellite Infrared Radiation Data. P. Krishna Rao, July 1970, 11 pp. (PB-194-685)

NESC 56 Time-Longitude Sections of Tropical Cloudiness (December 1966-November 1967). J. M. Wallace, July 1970, 37 pp. (COM-71-00131)

NOAA Technical Reports

NESS 55 The Use of Satellite-Observed Cloud Patterns in Northern Hemisphere 500-mb Numerical Analysis. Roland E. Nagle and Christopher M. Hayden, April 1971, 25 pp. plus appendixes A, B, and C. (COM-73-50262)

NESS 57 Table of Scattering Function of Infrared Radiation for Water Clouds. Giichi Yamamoto, Masayuki Tanaka, and Shoji Asano, April 1971, 8 pp. plus tables. (COM-71-50312)

NESS 58 The Airborne ITPR Brassboard Experiment. W. L. Smith, D. T. Hilleary, E. C. Baldwin, W. Jacob, H. Jacobowitz, G. Nelson, S. Soules, and D. Q. Wark, March 1972, 74 pp. (COM-72-10557)

NESS 59 Temperature Sounding From Satellites. S. Fritz, D. Q. Wark, H. E. Fleming, W. L. Smith, H. Jacobowitz, D. T. Hilleary, and J. C. Alishouse, July 1972, 49 pp. (COM-72-50963)

NESS 60 Satellite Measurements of Aerosol Backscattered Radiation From the Nimbus F Earth Radiation Budget Experiment. H. Jacobowitz, W. L. Smith, and A. J. Drummond, August 1972, 9 pp. (COM-72-51031)

NESS 61 The Measurement of Atmospheric Transmittance From Sun and Sky With an Infrared Vertical Sounder. W. L. Smith and H. B. Howell, September 1972, 16 pp. (COM-73-50020)

NESS 62 Proposed Calibration Target for the Visible Channel of a Satellite Radiometer. K. L. Coulson and H. Jacobowitz, October 1972, 27 pp. (COM-73-10143)

NESS 63 Verification of Operational SIRS B Temperature Retrievals. Harold J. Brodrick and Christopher M. Hayden, December 1972, 26 pp. (COM-73-50279)

NESS 64 Radiometric Techniques for Observing the Atmosphere From Aircraft. William L. Smith and Warren J. Jacob, January 1973, 12 pp. (COM-73-50376)

NESS 65 Satellite Infrared Soundings From NOAA Spacecraft. L. M. McMillin, D. Q. Wark, J.M. Siomkajlo, P. G. Abel, A. Werbowetzki, L. A. Lauritson, J. A. Pritchard, D. S. Crosby, H. M. Woolf, R. C. Luebbe, M. P. Weinreb, H. E. Fleming, F. E. Bittner, and C. M. Hayden, September 1973, 112 pp. (COM-73-50936/6AS)

NESS 66 Effects of Aerosols on the Determination of the Temperature of the Earth's Surface From Radiance Measurements at 11.2 m. H. Jacobowitz and K. L. Coulson, September 1973, 18 pp. (COM-74-50013)

NESS 67 Vertical Resolution of Temperature Profiles for High Resolution Infrared Radiation Sounder (HIRS). Y. M. Chen, H. M. Woolf, and W. L. Smith, January 1974, 14 pp. (COM-74-50230)

NESS 68 Dependence of Antenna Temperature on the Polarization of Emitted Radiation for a Scanning Microwave Radiometer. Norman C. Grody, January 1974, 11 pp. (COM-74-50431/AS)

NESS 69 An Evaluation of May 1971 Satellite-Derived Sea Surface Temperatures for the Southern Hemisphere. P. Krishna Rao, April 1974, 13 pp. (COM-74-50643/AS)

NESS 70 Compatibility of Low-Cloud Vectors and Rawins for Synoptic Scale Analysis. L. F. Hubert and L. F. Whitney, Jr., October 1974, 26 pp. (COM-75-50065/AS)

NESS 71 An Intercomparison of Meteorological Parameters Derived From Radiosonde and Satellite Vertical Temperature Cross Sections. W. L. Smith and H. M. Woolf, November 1974, 13 pp. (COM-75-10432/AS)

NESS 72 An Intercomparison of Radiosonde and Satellite-Derived Cross Sections During the AMTEX. W. C. Shen, W. L. Smith, and H. M. Woolf, February 1975, 18 pp. (COM-75-10439/AS)

NESS 73 Evaluation of a Balanced 300-mb Height Analysis as a Reference Level for Satellite-Derived soundings. Albert Thomasell, Jr., December 1975, 25 pp.

NOAA--S/T 76-2164